



Thiazole-pyrazoline hybrids as potential antimicrobial agent: Synthesis, biological evaluation, molecular docking, DFT studies and POM analysis



Rezan Huseen Hama Salih^a, Aso Hameed Hasan^{a,b,1,*}, Narmin Hamaamin Hussien^c, Farouq Emam Hawaiz^d, Taibi Ben Hadda^{e,f,1}, Joazaizulfazli Jamalish^{b,1}, Faisal A. Almalki^f, Adedapo S. Adeyinka^g, Louis-Charl C. Coetzee^g, Abel Kolawole Oyebamiji^h

^a Department of Chemistry, College of Science, University of Garmian, Kalar, Kurdistan Region-Iraq 46021, Iraq

^b Department of Chemistry, Faculty of Science, Universiti Teknologi Malaysia, Johor Bahru, Johor 81310, Malaysia

^c Department of Pharmacognosy and Pharmaceutical Chemistry, College of Pharmacy, University of Sulaimani, Sulaimani 46001, Iraq

^d Department of Chemistry, College of Education, Salahaddin University, Erbil, Kurdistan Region-Iraq 44001, Iraq

^e Laboratory of Applied Chemistry & Environment, Faculty of Sciences, Mohammed Premier University, Oujda 60000, Morocco

^f Department of Pharmaceutical Chemistry, Faculty of Pharmacy, Umm Al-Qura University, Makkah 21955, Saudi Arabia

^g Department of Chemical Sciences, University of Johannesburg, P.O. Box 524, Auckland Park 2006, South Africa

^h Industrial Chemistry Programme, Bowen University, Iwo, Nigeria

ARTICLE INFO

Article history:

Received 18 November 2022

Revised 13 January 2023

Accepted 16 February 2023

Available online 20 February 2023

Keywords:

Thiazole

Pyrazoline

Antimicrobial

Pom theory

Pharmacophore sites identification

DFT

HOMO-LUMO

ABSTRACT

In this study, an efficient synthesis of new thiazole-pyrazoline hybrids was investigated and hybrids were screened for their antimicrobial activities against four species of pathogenic bacteria and one fungal strain utilizing the well-diffusion and MIC assays using ciprofloxacin and fluconazole as the positive controls. The obtained results revealed excellent to moderate antibacterial and antifungal activity. Among them, compound **11b** showed potent antibacterial activity against *A. baumannii* with MIC of 16 µg/mL, while ciprofloxacin was ineffective. Molecular docking studies showed that compound **11b** had a stronger binding affinity of about 1 kcal/mol to gram-positive and gram-negative bacteria than compared with compound **11a**. Furthermore, the results of the POM (Petra, Osiris, Molinspiration) bioinformatics investigations show that the two studied heterocycles present a very good non toxicity profile, a bad bioavailability, and pharmacokinetics. Finally, an antibacterial pharmacophore (N^{δ-}, HN^{δ-}) and two antifungal pharmacophores (N^{δ-}, S^{δ-}) and (N^{δ-}, N^{δ-}) were evaluated in the POM investigations and deserves all our attention to be tested against other pathogenic microorganisms. The more potent compound **11b** compared to that of **11a** can also be attributed to its lower HOMO-LUMO gap which is an indicator of greater reactivity.

© 2023 Elsevier B.V. All rights reserved.

1. Introduction

Heterocyclic analogs have received continuous attention from scientists over the years due to their promising pharmacological characteristics [1–3]. They were developed as active agents in the design and discovery of new drug candidates [4,5]. Interestingly, heterocyclic compounds containing oxygen, nitrogen and sulfur atoms such as thiazoles and pyrazolines are considered as a basic platform for the building blocks of newer entities in medicinal chemistry [6]. The former are five-membered heterocyclic com-

pounds that contains a nitrogen and a sulfur (or an oxygen) atom [7], while the latter are five-membered heterocyclic compounds that contains two nitrogen atoms [8,9] (Fig. 1). The aromaticity of sulfur thiazoles is driven by the delocalization of non-bonding electron pairs from electron donating sulfur atoms to electron withdrawing nitrogen atoms to fulfill Huckle's rule (Fig. 2). The structural pattern of thiazole derivatives can be activated by substituting hydrogen atoms with desirable moieties at positions 2, 4 and 5. To synthesize a thiazole compound, the Hantzsch synthesis still remains the most convenient method, although other methods such as Cook-Heilbron synthesis and Gabriel synthesis has also been used. Although the Hantzsch synthesis is the most convenient method, it often produces low yields. These prompted researchers to search for methods that can produce higher yields. Aldehydes or ketones are generally used as reagents in condensation reactions

* Corresponding author at: Department of Chemistry, College of Science, University of Garmian, Kalar, Kurdistan Region-Iraq 46021, Iraq.

E-mail address: aso.hameed@garmian.edu.krd (A.H. Hasan).

¹ All these coauthors participated equally to this research.

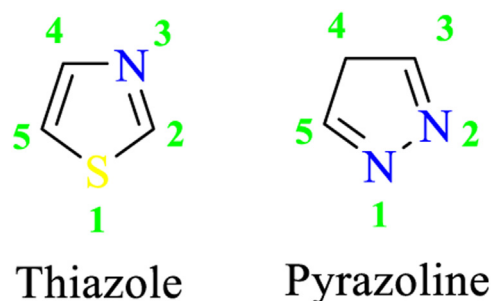


Fig. 1. Generic structures of thiazole and pyrazoline compounds.

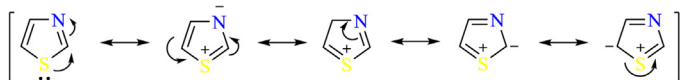


Fig. 2. Resonance structures of the thiazole ring.

with primary amines in ethanol or methanol in the synthesis of thiazoles [7]. The synthesis of pyrazoles can be achieved through various methods which includes, ultrasonic irradiation, microwave irradiation, ionic liquid, grinding technique and the conventional condensation method. Pyrazolines can be produced in a two stage process where the first stage involves the Claisen-Schmidt condensation reaction between acetophenone and aldehyde analogs to produce the desired α , β -enone. The second stage then involves the reaction between the α , β -enone and a hydrazine or a diazoalkane. The pyrazoline structure is an active site that can provide many biological activities [8,10].

Thiazole and pyrazoline derivatives can be effectively used as potential anti-microbial [2,11–14], anti-cancer [15–18], antiviral [19], anti-inflammatory [20–22], anti-oxidant [23] agents. Some of these compounds have also shown anti-cholinesterase [24,25], anti-malarial [2,26], and anti-analgesic [27,28] properties. Fig. 3 shows thiazole and pyrazole compounds where (4-(4-bromophenyl)-2-(pyridin-4-yl)thiazole **1** acted as a potent antibacterial inhibitor [11]. Mor et al. combined thiazole and pyrazole pharmacophore moieties in one molecular scaffold and assayed it for inhibitory activity against various bacterial and fungal strains. Among the tested compound, **2** was the found to be the most potent inhibitor [29]. In another study, Asad and co-workers successfully synthesized a series of novel *N*-trifluoroacetyl-2-pyrazolines and evaluated them for their antibacterial activity against *E. coli* and *P. aeruginosa*. From these tests, Compound **3** exhibited significant inhibitory activity [12]. Eissa et al. have reported derivative containing thiazole core **4** as promising anti-fungal agents [30].

In light of the above-mentioned findings, we expected that these two active pharmacophores would produce new thiazole-pyrazoline hybrids to act as potent novel anti-microbial agents for pharmacological activities against four bacterial strains (*Staphylococcus aureus*, *Escherichia coli*, *Pseudomonas aeruginosa*, and *Acinetobacter baumannii*) and one fungal strain (*Candida albicans*). Computational investigation of their structure and reactivity was also carried out via conceptual density functional theory (CDFT), molecular docking studies and POM (Petra/Osiris/Molinspiration) analysis in order to identify the factors responsible for their relative biological activity towards the various bacterial strains.

2. Results and discussion

2.1. Chemistry

1-(4-((4-chlorobenzyl)oxy)phenyl)ethan-1-one **7** was prepared in excellent yield (97%) based on Williamson synthesis of ether

by direct benzoylation of *para*-hydroxy acetophenone **5** with 4-chlorobenzylchloride **6**, in the presence of anhydrous potassium carbonate in ethanol. The synthesis of pyrazoline derivatives (**9a-b**) accomplished via the condensation reaction of compound **7**, substituted benzaldehydes (**8a-b**) with thiosemicarbazide in dilute ethanolic sodium hydroxide solution [31]. Treatment of derivatives (**9a-b**) with bromophenacylbromide **10** in boiled ethanol afforded titled compounds (**11a-b**) (Scheme 1).

The structures of synthesized thiazoles (**11a-b**) were characterized by FT-IR, ^1H NMR, ^{13}C NMR, and UV-Vis. spectroscopic measurement. The FT-IR data of condensed thiazoles (**11a-b**) showed two bands at (1591–1602) cm^{-1} and (1552–1512) cm^{-1} attributed to C=C and C=N stretching vibrations, respectively. Moreover, the disappearance of (NH₂) stretching vibrations of the carbothioamide group attached to the pyrazoline ring at (3400–3200) cm^{-1} was very informative and good evidence for the formation of thiazole rings in the desired compounds. The ^1H NMR spectra of thiazoles (**11a-b**), displayed three doublet to doublets (dd) peaks, because of the ABX spin system, which is the result of nonequivalence of three protons attached to the C₁₁ and C₁₂ carbon atoms of the pyrazoline ring. The ^1H NMR spectral measurement of thiazole (**11a**), showed three (dd) doublet to doublet signals at (3.29, 3.86 and 5.60) ppm for (-CH₂-H_a-C₁₁, -CH₂-H_b-C₁₁ and -CH-H_x-C₁₂) consequently, also three singlet signals to (-O-CH₂-C₁₇, -O-CH₂-C₅ and -CH-C₂₄) groups were appeared at (5.01, 5.10 and 6.81) ppm respectively, and the other peaks between (6.92–7.73) for aromatic hydrogen atoms. Whereas, the ^1H NMR spectrum of thiazole (**11b**), exhibited three (dd) doublet to doublet signals at (3.32, 3.87 and 5.59) ppm for (-CH₂-H_a-C₁₁, -CH₂-H_b-C₁₁ and -CH-H_x-C₁₂) consequently. On the other hand, three singlet signals to (-O-CH₂-C₁₉, -O-CH₂-C₅ and -CH-C₂₈) groups were appeared at (5.02, 5.08 and 6.77) ppm respectively, and the other signals between (6.86–8.25) for 20 aromatic protons

The ^{13}C NMR spectra of thiazole compounds (**11a-b**) showed four characteristic peaks in the high field region corresponding to (C₁₁, C₁₂, C₁₇ and C₅) and (C₁₁, C₁₂, C₁₉ and C₅) carbon atoms at [(43.51, 64.05, 69.22 and 69.28) and (43.56, 64.42, 68.69 and 69.33)] ppm for each compound (**11a-b**) respectively. A characteristic band at (165.15 and 165.12) ppm attributed to (S=C=N) (C₂₂ and C₂₆) carbon atoms for each synthesized compound (**11a-b**) confirm the expected structure of thiazole ring. The UV-Vis. spectra of synthesized thiazoles (**11a-b**) show a blue shift with respect to λ_{max} of the reactant pyrazolines (**9a-b**) in the range (294–360) nm, since it gave λ_{max} in the range (218–254) nm, which is attributed to cyclization of thiocarbamyl group.

2.2. Antibacterial and antifungal activities

The antibacterial and antifungal activities of synthesized compounds (**11a-b**) were evaluated *in vitro* against *S. aureus*, *E. coli*, *P. aeruginosa*, *A. baumannii* and *C. albicans*. The newly synthesized compounds were evaluated as antibacterial and antifungal references, in comparison to ciprofloxacin and fluconazole. The results of the antimicrobial activity tests and the minimum inhibitory concentrations (MICs) of compounds (**11a-b**) are summarized in Fig. 4 and Table 1. Compound **11b** showed interesting antibacterial activity at the concentration used, in particular against *E. coli*, *A. baumannii*, *S. aureus* and *P. aeruginosa* with inhibition diameters of 25, 23, 22 and 22 mm, respectively, compared to ciprofloxacin with zones of inhibition of 28, 30 and 28 mm diameter, while ciprofloxacin was ineffective against *A. baumannii*.

The MIC for **11b** showed inhibition at 16 $\mu\text{g}/\text{mL}$ against *S. aureus*, *E. coli* and *A. baumannii*, however, *S. aureus* had a smaller standard error of 0.022 than the other bacterial strains. Also, compound **11b** showed potent antibacterial activity against *P. aeruginosa* at 8 $\mu\text{g}/\text{mL}$, and the standard error was 0.012. Furthermore,

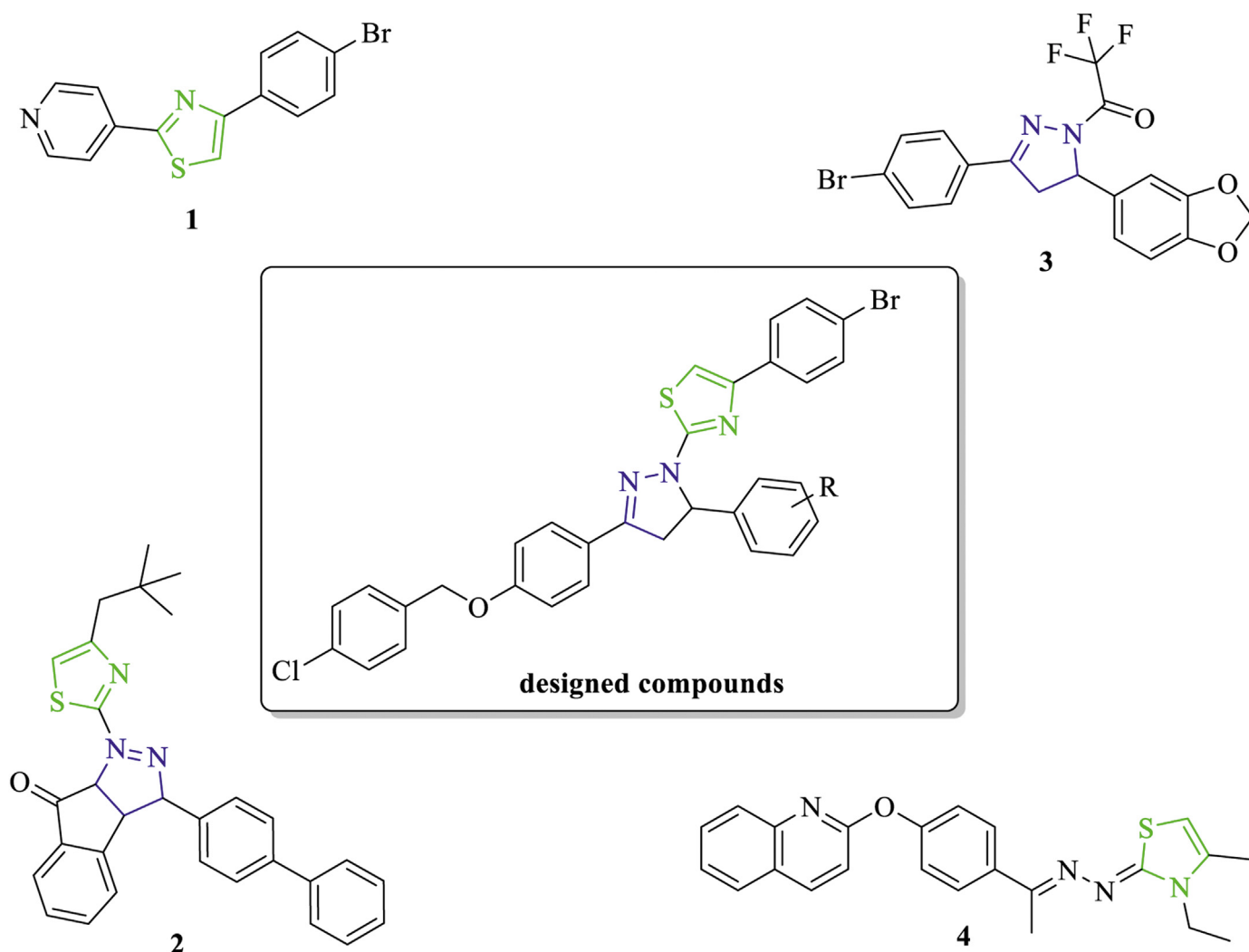


Fig. 3. Reported antimicrobial inhibitors which contain pharmacophores such as thiazole, pyrazoline and our newly designed compounds.

Table 1

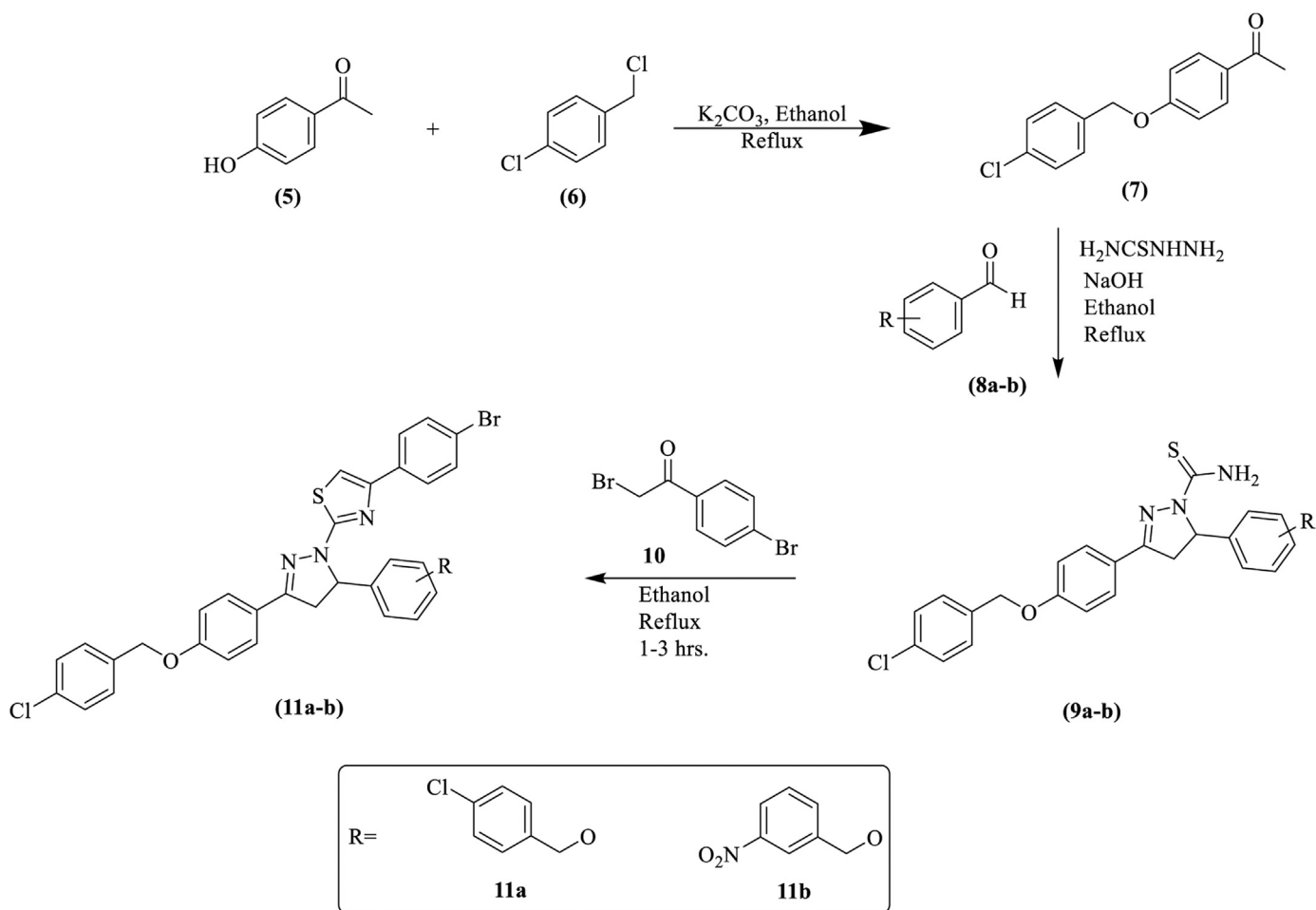
The MIC values in $\mu\text{g/mL}$ exhibited by the tested compounds (**11a-b**) against selected species of microorganisms using the microplate serial dilution method.

Compounds	MIC values in $\mu\text{g/mL}$ expressed by the test compound				
	Bacterial strains				Fungi
	<i>Staphylococcus aureus</i>	<i>E. coli</i>	<i>Pseudomonas aeruginosa</i>	<i>Acinetobacter baumannii</i>	<i>Candida albicans</i>
11a	32	16	16	32	32
11b	16	16	8	16	32
Ciprofloxacin	4	0.5	0.5	-	-
Fluconazole	-	-	-	-	16

compound **11a** showed a good antibacterial activity against *E. coli*, *A. baumannii*, *S. aureus* and *P. aeruginosa* with inhibition diameters of 24, 21, 20 and 19 mm respectively. The MIC for **11a** highly inhibited *E. coli* and *P. aeruginosa* at 16 $\mu\text{g/mL}$, and the standard errors were 0.024 and 0.027 respectively.

On the other hand, the antifungal results shown in Table 1, the antifungal activities of compounds (**11a-b**), showed considerable antifungal activity against *C. albicans* with 12- and 16-mm diameter zones of inhibition, respectively, compared to fluconazole with 24 mm diameter zone of inhibition. The MIC for (**11a-b**) against *C. albicans* showed inhibition at 32 $\mu\text{g/mL}$. The standard error for **11a** was 0.024. Based on the antibacterial and antifungal results listed in Table 1, it may be concluded that compounds (**11a-b**) exhibited a broad spectrum of antibacterial activity against all tested.

Regarding the derivatives (**11a-b**), it was found that the presence of an electron-withdrawing group on the terminal phenyl ring of the pyrazoline moiety enhanced the antibacterial activity. Replacing the chlorine atom at the para position with nitro at the meta position enhanced the antibacterial activity and the meta position was preferred. The nitro atom is also superior to the halogens for monosubstituted derivatives in terms of effectiveness, since it has a higher electronegativity. In addition, with respect to SAR studies of synthesized compounds as antibacterial agents, it was discovered that there is no specific substituent on the phenyl ring directly bonded to the pyrazoline nucleus of compounds (**11a-b**). This could determine the activity of electron withdrawing groups and enhanced antibacterial activity to be attributed to the improvement of the physicochemical properties and thus, to the im-



Scheme 1. Synthesis of hybrids (11a-b).

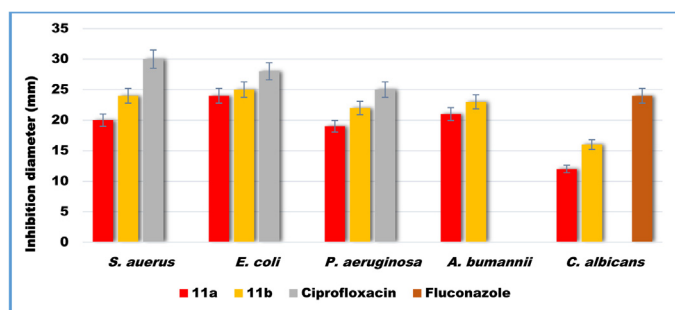


Fig. 4. Antimicrobial activity of hybrids (11a-b) in comparison with the antibiotic ciprofloxacin and antifungal fluconazole.

provement of the permeability of the bacterial cells. Regarding SAR studies for antifungal activities of the newly synthesized derivatives, it was found that the presence of an electron-withdrawing group on the terminal phenyl ring of the pyrazoline moiety enhances the antifungal activity, and para or meta position is optimal for the antifungal activity for monosubstituted derivatives.

2.3. Molecular docking analysis

The selected two thiazole-pyrazoline hybrids docked against Tyrosyl-tRNA synthetase (PDB ID: 1jjj) (gram- positive bacteria) [32], Type IIA topoisomerase (PDB ID: 2xct) (gram- negative bacteria) and CYP51 (PDB: 3juv) (sterol 14-alpha demethylase) [33] re-

Table 2

Calculated binding affinity for compound (11a-b) against the studied receptors.

Compounds		Binding Affinity (kcal/mol)		
		(PDB ID: 1jjj)	(PDB ID: 2xct)	(PDB: 3juv)
11a		-10.0	-9.4	-8.3
11b		-10.9	-9.3	-9.4
Positive controls	Ciprofloxacin	-7.3	-6.4	-
	Fluconazole	-	-	-7.1

sulted to series of values (binding affinity) that revealed the potency of the studied compounds. As shown in Table 2, the calculated binding affinity for synthesized compounds (11a-b) against Tyrosyl-tRNA synthetase (PDB ID: 1jjj) were -10 kcal/mol and -10.9 kcal/mol, against Type IIA topoisomerase (PDB ID: 2xct) were -9.4 kcal/mol and -9.3 kcal/mol, and against CYP51 (sterol 14-alpha demethylase) (PDB: 3juv) were -8.3 kcal/mol and -9.4 kcal/mol. It was reported that the lower the binding affinity value, the better the inhibiting activity [34,35]; thus, compound 11b with -10.9 kcal/mol and -9.4 kcal/mol proved to have greater tendency to inhibit Tyrosyl-tRNA synthetase and CYP51 (sterol 14-alpha demethylase) than 11a (Figs. 5-7). However, as reported in Table 2, compound 11a proved to be a potential Type IIA topoisomerase inhibitor and this proved that its inhibiting activity was more potent than the activity of 11b against Type IIA topoisomerase (Fig. 6). The inhibiting activity of the docked selected compounds were compared with the inhibiting activity of the referenced drug used in this research; therefore, the selected com-

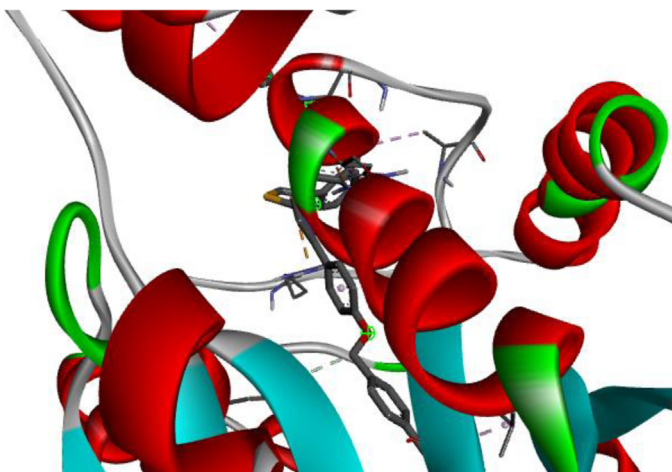


Fig. 5. 3D structure of **11b**-Tyrosyl-tRNA synthetase (PDB ID: 1jjj) complex.

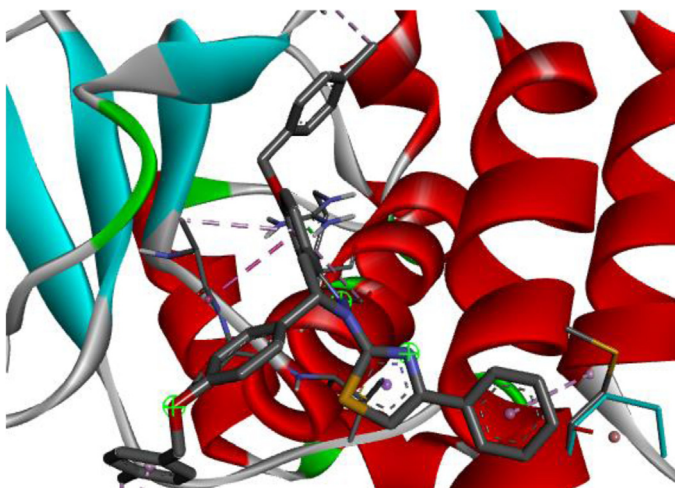


Fig. 6. 3D structure of **11a**-Type IIA topoisomerase (PDB ID: 2xtc) complex.

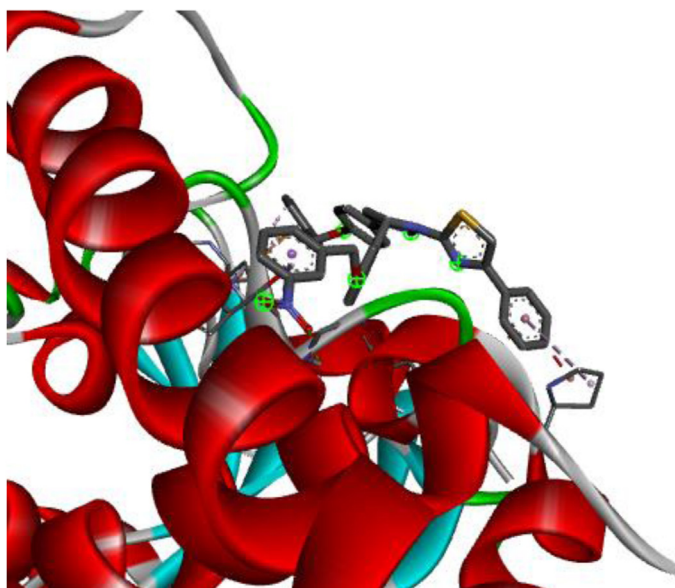


Fig. 7. 3D structure of **11b**-CYP51 (sterol 14-alpha demethylase) (PDB: 3juv) complex.

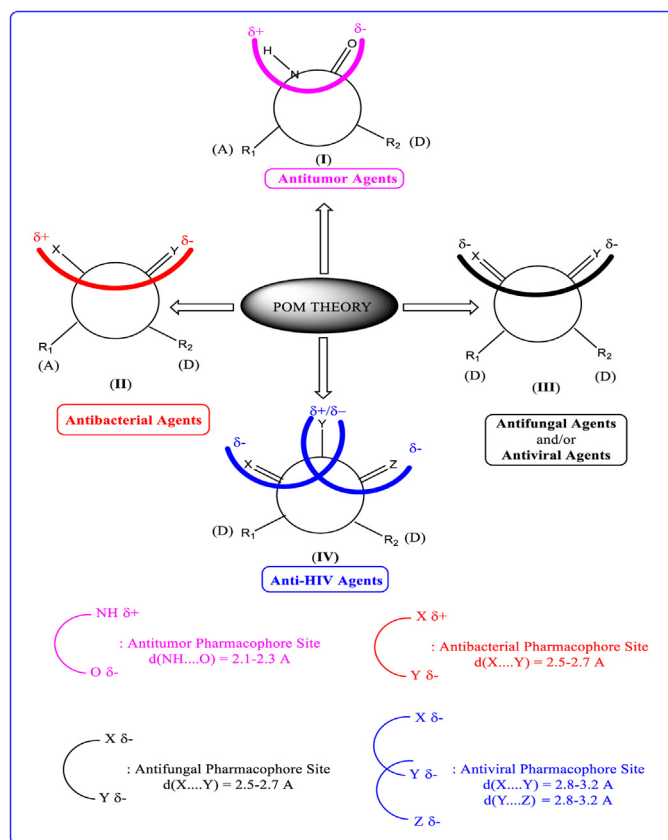


Fig. 8. The concept and applications of POM Theory in the identification and optimization of pharmacophore sites of various classes of drugs, was developed with success by Prof. T. Ben Hadda (Principal Inventor of POM Theory) in collaboration with NCI and TAACF of the USA [32].

compounds (**11a-b**) proved to be more potent in inhibiting Tyrosyl-tRNA synthetase, Type IIA topoisomerase (as well as CYP51 (sterol 14-alpha demethylase) than the referenced drugs.

2.4. POM analyses of compounds (11a-b)

POM Theory (Petra/Osiris/Molinspiration) that is invented by group of Taibi Ben Hadda in collaboration with the American NCI and TAACF, led us to a real success in pharmacology and drug design fields [36,37]. Here we treat the series of the tested compounds (**11a-b**) in the goal to identify their pharmacophore sites, according to the POM organigram (Fig. 8).

So the two compounds (**11a-b**) were also screened for the *in-silico* POM study to calculate various general properties along with the prediction of antibacterial/antifungal bioactivity [36,37]. Data were analyzed and compared with standard anti-microbial drugs. Osiris and Molinspiration are two cheminformatic-based software tools that help in the calculation of toxicity risks and molecular properties as well as in the forecasting of bioactivity scores of the screened compounds [38,39]. As our tested compounds (**11a-b**) have a molecular weight of more than 500 g/mol, they may be slowly absorbed because most of the traded drugs (i.e., approximately 80% of them) have molecular weights in this range (Table 3). This directly impacts compounds (**11a-b**), which have a negative drug score. The drug-likeness of compounds (**11a-b**) are -4.16 and -0.80 , respectively, and their drug scores are low limited to 5–8%, respectively (Table 3).

From Molinspiration data (Table 4), it was concluded that the series of tested compounds (**11a-b**) doesn't satisfy the rule of Lipinski and needs more work on their properties. The cLogP value of

Table 3
Osiris analysis of compounds (**11a-b**).

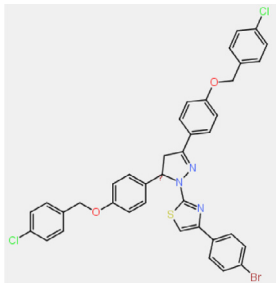
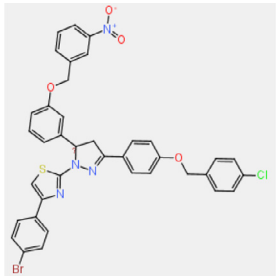
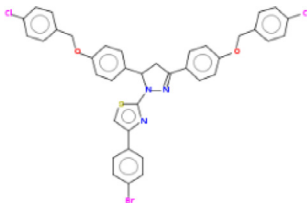
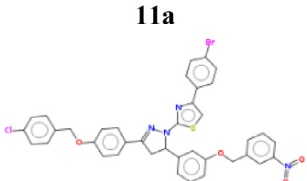
Compd	Molecular Structure	Toxicity Risks	Solubility	Drug-Score
(11a)		Toxicity Risks ● mutagenic [?] ● tumorigenic [?] ● irritant [?] ● reproductive effective [?]	cLogP [?] 11.13 Solubility [?] -11.06 Molweight 739.0	TPSA [?] 75.19 Druglikeness [?] 4.16 Drug-Score [?] 0.08
(11b)		Toxicity Risks ● mutagenic [?] ● tumorigenic [?] ● irritant [?] ● reproductive effective [?]	cLogP [?] 9.43 Solubility [?] -10.7 Molweight 750.0	TPSA [?] 121.0 Druglikeness [?] -0.8 Drug-Score [?] 0.05

Table 4
Molinspiration analysis of compounds (**11a-b**).

Compound	Molecular Properties	Bioactivity Scores
 11a	cLogP 9.49 TPSA 46.96 MW 741.54 nOHNH 0 nviolations 2 volume 583.00	GPCR ligand -0.65 Ion channel modulator -1.44 Kinase inhibitor -0.98 Nuclear receptor ligand -0.92 Protease inhibitor -0.56 Enzyme inhibitor -0.84
 11b	cLogP 9.30 TPSA 92.79 MW 752.09 nOHNH 0 nviolations 2 volume 592.80	GPCR ligand -0.92 Ion channel modulator -1.77 Kinase inhibitor -1.31 Nuclear receptor ligand -1.25 Protease inhibitor -0.77 Enzyme inhibitor -1.14

the compounds (**11a-b**) doesn't fall in the standard range, (i.e., less than 5); therefore, these compounds may be highly hydrophobe and, thus, do not meet the criteria of market drugs because all of their bioactivity scores are negative (Table 4).

2.5. Identification of antibacterial/antifungal pharmacophore sites of (11a-b)

The invention of POM Theory leads us to identify each type of pharmacophore site with real success on the basis of semi-empirical data of about 7.000 antibacterial, antifungal, antitumor and antiviral commercial and known and new drugs. All details of therapeutic applications of POM Theory are given in the literature, and the identification of different and various types of pharmacophore sites is well established [36–43] with real success.

The atomic charge calculation of compounds (**11a-b**) (Table 4) show that all nitrogen and sulfur atoms are negatively charged

(Fig. 9). The distance between any couple of two heteroatoms can be obtained after optimization of molecular structure (Fig. 9 and Table 5). The Nitrogen atom (N2) is the most negatively charged. So, it plays a crucial role in regenerating two combined ($N2^{\delta-}-N1^{\delta-}$) and/or ($N2^{\delta-}-S1^{\delta-}$) antifungal pharmacophore sites. The rest of the substituents are overdose. They are less interesting and certainly not needed here. Excess of substituents has a poor impact on the bioavailability.

The number of antifungal pharmacophore sites is now well determined, but what about the antibacterial pharmacophore sites?

To reply to the query given above, we should take into consideration that bacteria regenerate folic acid, which constitutes an evident source of protonation of compounds (**11a-b**), as shown in Fig. 10.

So the identification of Pharmacophore sites of compounds (**11a-b**) based on the atomic charge of optimized structures (Figs. 9–10) confirms our hypothesis (Fig. 11).

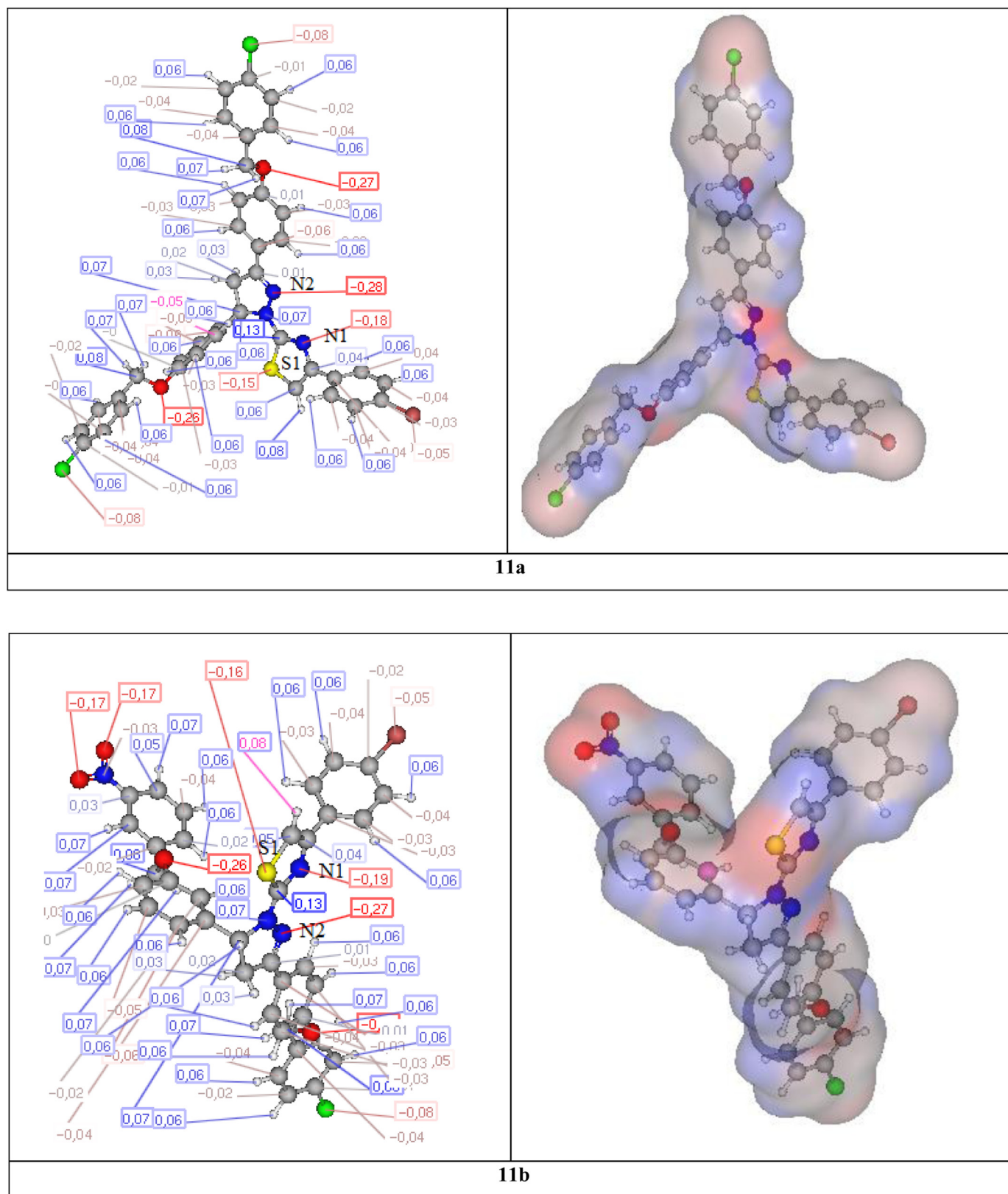


Fig. 9. Atomic charge of compounds (11a-b).

Table 5
Atomic charge of Nitrogen and Sulfur atoms of the antifungal (N2^{δ-}-N1^{δ-}) and (N2^{δ-}-S1^{δ-}) pharmacophore sites of 11a-b.

Compd.	N1	N2	S1	Pharmacophore sites		Total of Antifungal Pharmacophore Sites
11a	-0.16	-0.28	-0.15	N2 ^{δ-} -N1 ^{δ-}	N2 ^{δ-} -S1 ^{δ-}	Two Antifungal Sites
11b	-0.19	-0.27	-0.16	N2 ^{δ-} -N1 ^{δ-}	N2 ^{δ-} -S1 ^{δ-}	Two Antifungal Sites

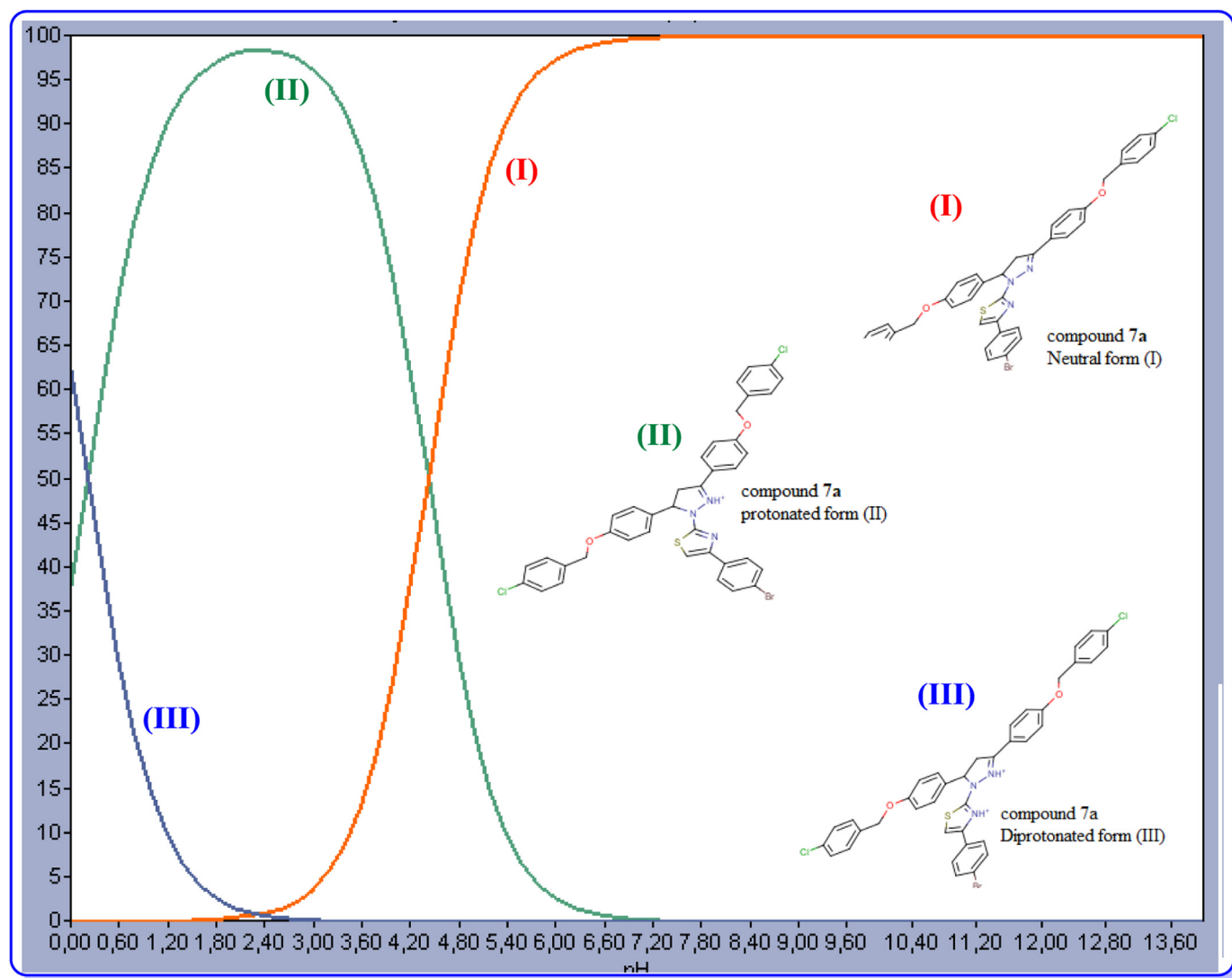


Fig. 10. Microspecies distribution (%) of compound 11a leading to bioactive metabolites.

2.6. DFT calculations

2.6.1. Frontier molecular orbitals

The chemical reactivity parameters were obtained using frontier molecular orbital (FMO) data reactivity descriptors such as chemical hardness (η), global softness (δ), ionization potential (IP), electron affinity (EA), electrophilicity index (ω), electronegativity (χ) etc. These parameters can be calculated using Koopman's theorem [44].

$$IP = (-E_{HOMO}) \quad (1)$$

$$EA = (-E_{LUMO}) \quad (2)$$

Mulliken theory [45] states that χ can be calculated as

$$\chi = \left(\frac{IP + EA}{2} \right) \quad (3)$$

while η and δ can be calculated as

$$\eta = \left(\frac{IP - EA}{2} \right) \quad (4)$$

$$\delta = \frac{1}{\eta} \quad (5)$$

The chemical potential (μ) can be calculated using the Parr and Pearson relation [46]

$$\mu = -\left(\frac{IP - EA}{2} \right) \quad (6)$$

The Parr and Yang theory [47] states that the electron-accepting tendency of a species can be measured by the electrophilicity index (ω)

$$\omega = \frac{\mu^2}{2\eta} \quad (7)$$

The maximum amount of electronic charge index (ΔN_{max}) can be calculated with the relation

$$\Delta N_{max} = \frac{-\mu}{\eta} \quad (8)$$

The resistance of an atom to charge transfer (CT) can be measured by η [48,49], while the ability of an atom or a group of atoms to receive electrons can be measured by δ [50], and ω predicts the stabilization energy when electrons are saturated, which can be used to estimate biological activities [46,51–53]. The latter is defined as the change in energy of an electrophile when it meets a suitable nucleophile [51,54–56]. An organic molecule can display both electrophilic and nucleophilic behavior, which can

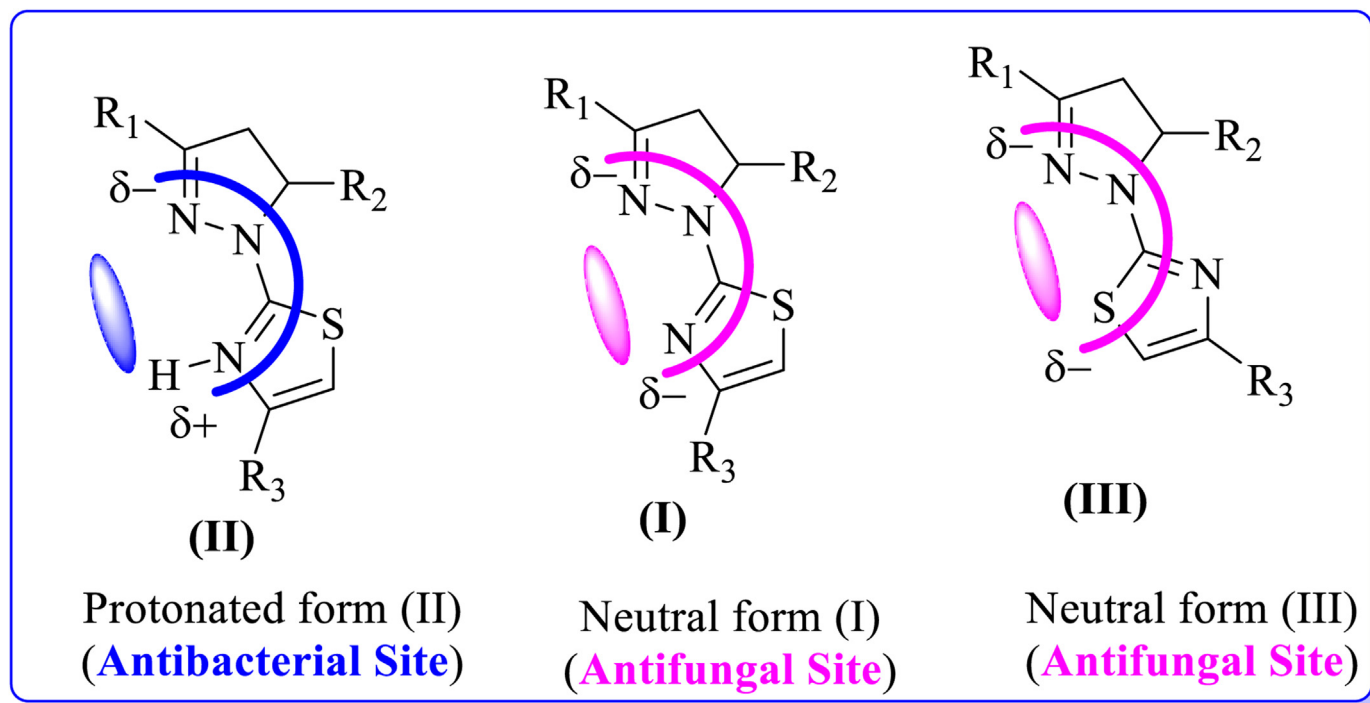


Fig. 11. Identification of closed antibacterial and antifungal pharmacophore sites.

Table 6

Comparisons of the energies for highest occupied molecular orbitals, lowest unoccupied molecular orbitals, energy gaps and Ionization Potentials for the compounds.

Compound	11a	11b
HOMO (eV)	-6.62	-6.71
LUMO (eV)	-0.74	-1.79
ΔE (eV)	5.87	4.92
Ionization Potential (eV)	6.31	6.39
Electron Affinity (A)	0.06	0.73
Electronegativity (χ)	3.18	3.56
Hardness (η)	6.25	5.66
Softness (δ) (1×10^{-2})	1.60	1.77
Electrophilicity index (ω)	0.81	1.12
Nucleophilicity index (N)	4.02	3.94
Chemical Potential (μ) in (eV)	-3.18	-3.56

be measured by the nucleophilicity index (N) [50]. The energy released when an electron fills up the lowest unoccupied molecular orbital (LUMO) can be measured by the EA of the electron accepting power of an accepting molecule [48]. The energy required to remove an electron from its highest occupied molecular orbital (HOMO) is denoted by IP , which is a measurement of the electron donating power of a donor molecule [57]. The HOMO-LUMO energy gaps usually determine the stability of a compound, with lower energy gaps resulting in more reactive compounds [58]. Previously it was believed that an electron that occupies the HOMO will automatically be excited to the LUMO, but this theory was debunked by Bulat et al., which investigated twelve compounds where only five amongst the twelve contained electrons that occupied the HOMO level that were excited to the LUMO level. The study observed that an electron's position in atomic space and the contour of the molecule also played roles in excitation processes [59]. Although this is the case, it is still generally accepted that HOMO-LUMO energy gaps plays a significant role in chemical stabilities and reactivities of many organic molecules [60]. Table 6 shows a lower HOMO-LUMO energy gap for **11b**, which results in a slightly larger IP . Its lower LUMO induces higher EA and lower

η means that it is less resistant to CT, which results in electrons becoming more saturated. Thus, it should have higher biological activities than **11a** because of its lower HOMO-LUMO gap.

2.7. Average localize ionization energy (ALIE)

The molecular topology can be used to reveal the average localized ionization energy (ALIE), which can provide information about local reactive sites on the molecule through resonance, thus, explaining the stability of the compound. ALIE can be expressed as

$$\langle ct \rangle \bar{I} \langle ot \rangle (r) = \frac{\sum_i \rho_i(r) |\varepsilon_i|}{\rho(r)} \quad (9)$$

As $\bar{I}(r)$ can be used to remove an electron at point r in atomic or molecular space, ρ is the electron density and ε_i is the energy of an electron in an orbital φ_i . Lower $\bar{I}(r)$ values indicates that electrons are weakly bound at point r and can be easily removed. Although $\bar{I}(r)$ has widespread uses such as revealing atomic shell structures, measuring electronegativities, predicting pK_a , quantifying local polarizability and hardness, the most important purpose is predicting reactive sites of electrophilic or radical attacks. This is revealed by the minima of ALIE on the van der Waals surface [61–63]. When performing an ALIE analysis on **11a**, minima 36 displayed the lowest $\bar{I}(r)$ value of 9.86 eV, which was found to be S17 and minima 19 in **11b** displayed the lowest $\bar{I}(r)$ value (9.94 eV), which was observed on C16 (Fig. 12).

2.8. Electron localization function (ELF)

Electron localization function (ELF) studies the empirical concepts of electron localization, specifically, the electron pair localization in the spirit of Lewis structures. ELF is defined as follows

$$ELF = \frac{1}{1 + x_\sigma^2} \quad (10)$$

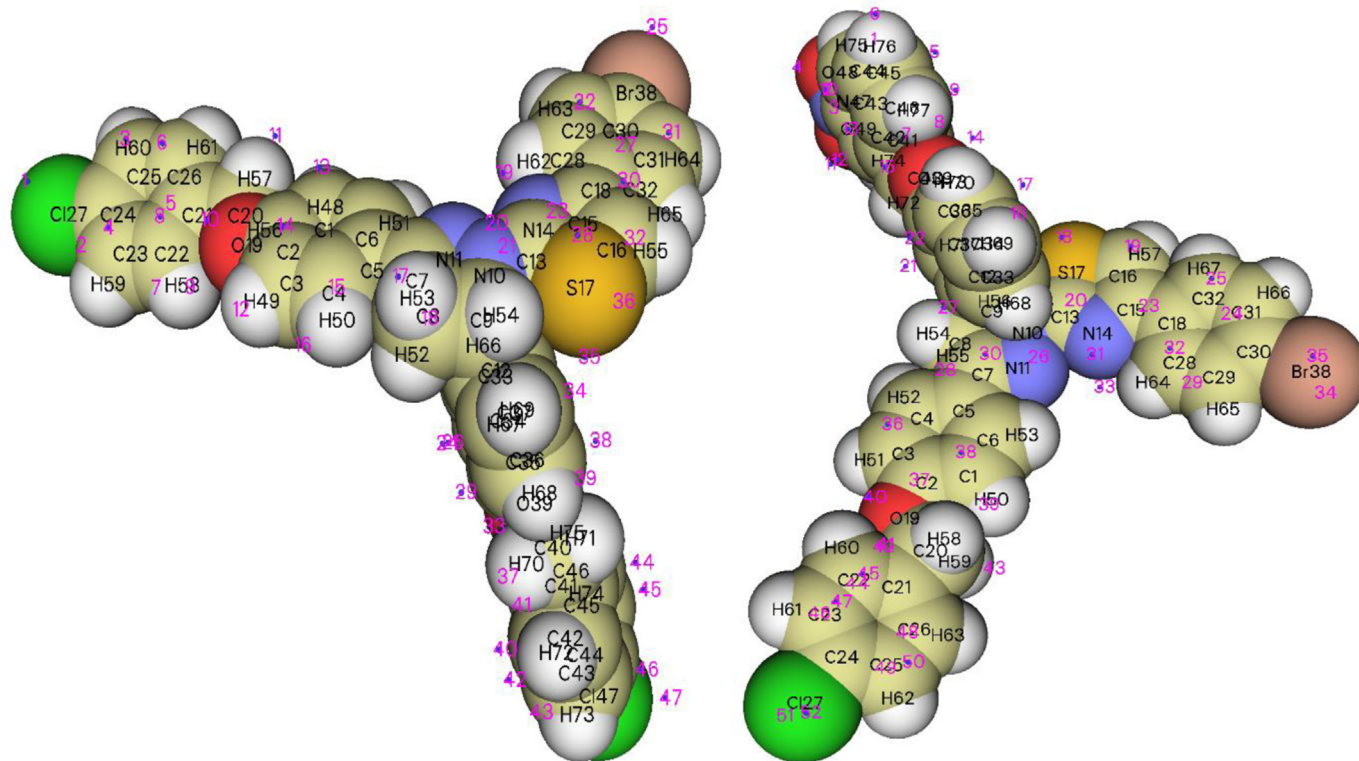


Fig. 12. Minimum ALIE indices for thiazoles.

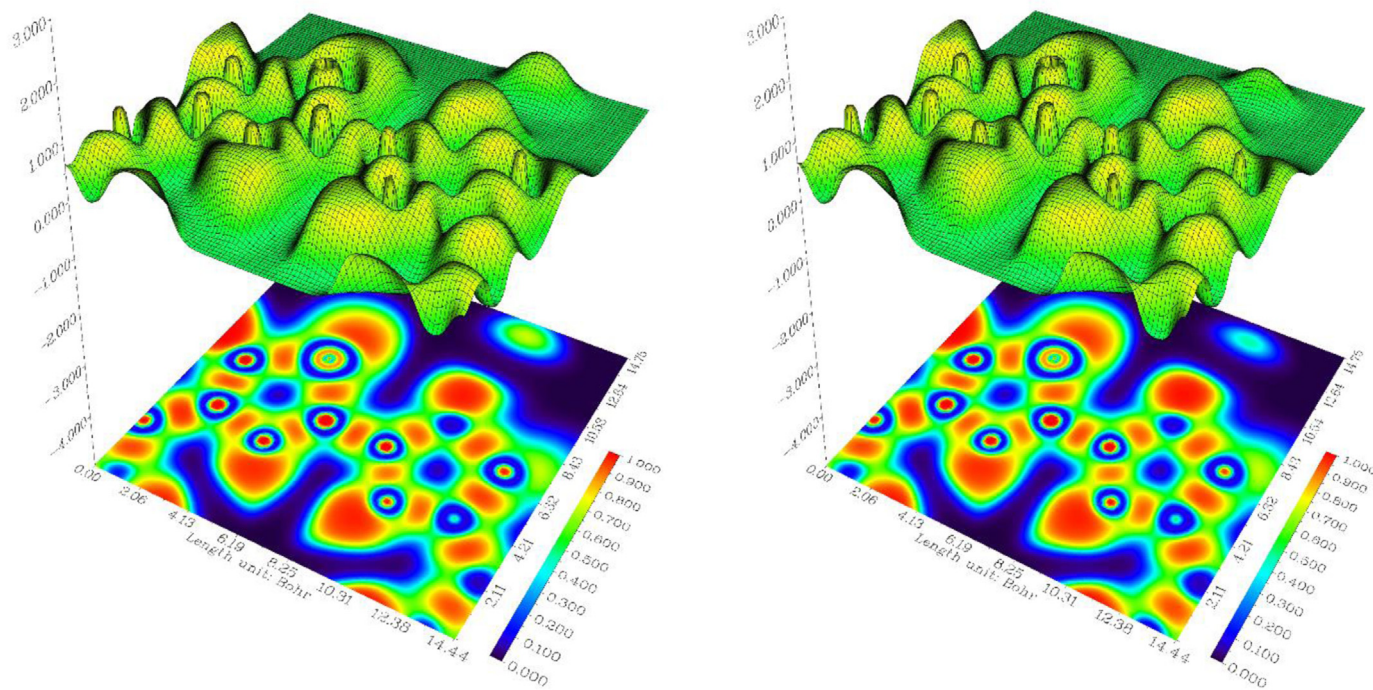


Fig. 13. Electron localization function of thiazoles across the N-C-S plane.

Where $x_{\sigma} = \frac{D_{\sigma}}{D_{\sigma}^0}$, which allowed ELF to obey the following inequality

$$0 \leq \text{ELF} \leq 1$$

An ELF value close to one correspond to a region in atomic space where electrons are highly localized, whereas a value close

to one-half correspond to gas like behavior [64]. Fig. 13 displays both two-dimensional and three-dimensional across the N10-C13-S17 plane. The red color indicates a high concentration of electrons across these atoms, while the blue color indicates that electrons are delocalized across these atoms. We observed that electrons are less localize at a length in the region 10.31–12.38 Bohr (in the x-direction) in **11b**.

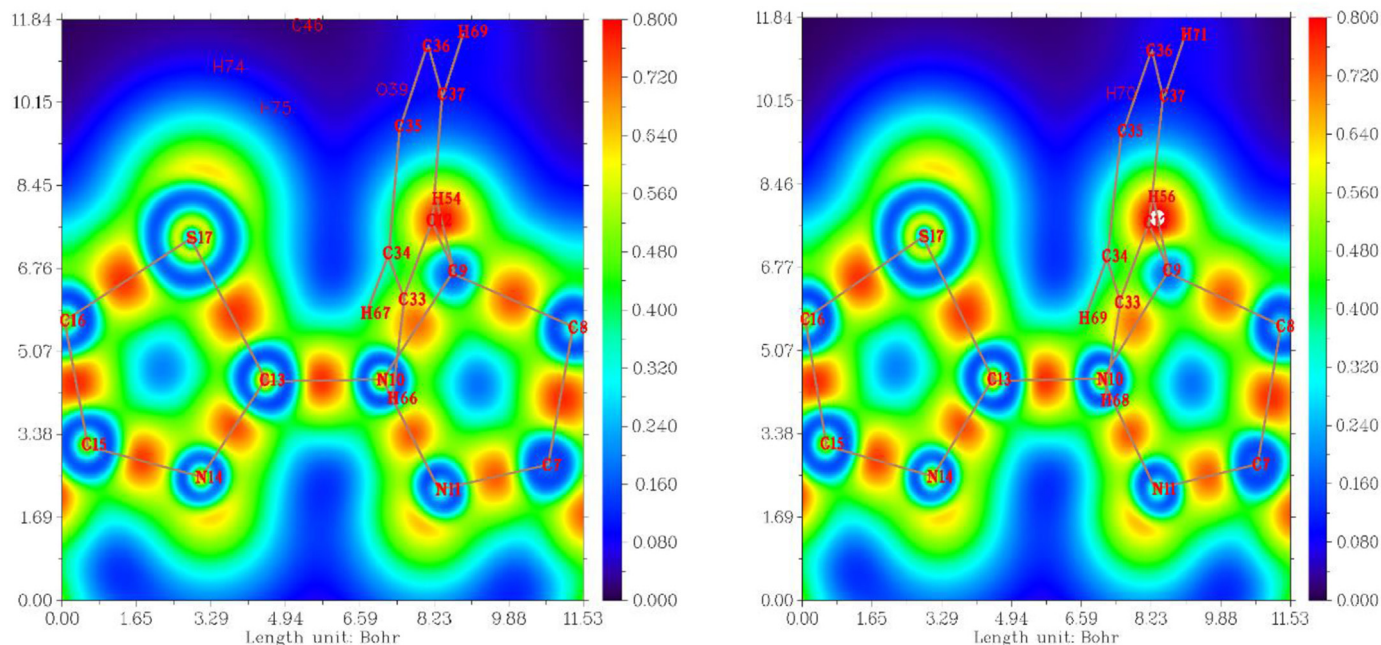


Fig. 14. Localize orbital locator of thiazoles across the N-C-S plane.

2.9. Localize orbital locator (LOL)

In addition to ELF, localize orbital locator (LOL) was also performed on the compounds. Although both ELF and LOL locate the regions of localized electrons, the latter simply recognises that gradients of localized orbitals are maximised when orbitals overlap [65]. Fig. 14 displays the localized orbital locator (LOL) regions for the thiazoles across the N-C-S planes where high electron localizations are observed between all the bonding regions.

2.10. Non-covalent-interactions (NCI)

Non-covalent-interactions (NCI) is a quantitative and qualitative tool that analyses the interactions that stabilizes compounds and can reveal information about the locations of these interactions. This descriptor uses a method based on electron density (ρ) calculations where it analyses the domains of weak ρ by obtaining low electron density gradients ($s(\rho)$), which identifies indices below the identification threshold of quantum theory of atoms in molecules (QTAIM) analysis. Loci of the space where the Reduced Electron Density Gradient (RDG) is close to zero and forms well-defined troughs is revealed by the NCI index (Fig. 15). These RDG regions are called isosurfaces and characterized by well-defined electron density values that arises from small gradients along each of them. To define a weak interaction, both s and ρ must be weak by definition. Red isosurfaces are caused by steric repulsion between atoms, while green and blue isosurfaces results from van der Waals attractive forces and hydrogen bonding. More intense colours result in stronger interactions. The strength of the interaction is measured by the index ρ , which is revealed by a well-defined trough, where the strongest interaction is revealed by the highest ρ . All forces are denoted by the eigenvalue λ_2 [66]. Although visible troughs for van der Waals attractive and repulsive interactions appears in Fig. 15, they do not appear as well-defined to indicate strong interactions. No hydrogen bonding interactions are also observed.

Three-dimensional NCI isosurfaces appears as red pill shapes, green/red sheets, and blue disks due to the closure of benzene rings, van der Waals attractive and repulsive forces and hydrogen

Table 7

Molecular electrostatic potential (MEP $\times 10^{-3}$) for the Thiazoles.

	11a	11b
N10	- 61.4	- 65.7
C13	- 69.6	- 34.4
S17	285	256

bonding [66] (Fig. 16). Other than hydrogen bonding, all these interactions were observed. This also verifies our observations for the two-dimensional isosurfaces.

As the critical points (CP) is defined as the gradient path where the ρ originates and terminates where the gradient path $\nabla\rho$ vanishes [67], it is observed that all the CPs arises from bonds between atoms and the closure of the benzene ring (Fig. 17).

2.11. Molecular electrostatic potential (MEP)

Molecular electrostatic potential (MEP) is a chemical descriptor that probes the electronegativities of atomic sites on molecules. Since electrostatic forces are primarily responsible for long range interactions, this descriptor is useful in rationalizing molecular recognition processes and molecular interactions [68]. A visual inspection was performed on the structures of these compounds to establish regions where nucleophilic or electrophilic attacks can occur with colours that includes red, orange, yellow, green, and blue (Fig. 18). These colours are an indication of the reduction potential on each atomic site and reduces in the order blue>green>yellow>orange>red. Thus, a blue region denotes a nucleophilic attack, while a red region denotes an electrophilic attack.

When we select the N-C-S plane (Fig. 19), we observe quantitative MEP measurements (Table 7) for these three atoms that makes up this plane. As the ALIE analysis showed that electrons on S17 in **11a** can be ionized more easily than electrons on S17 in **11b**, the quantitative values in Table 7 rationalized this further, as positive MEP values are more ionizable than negative MEP values.

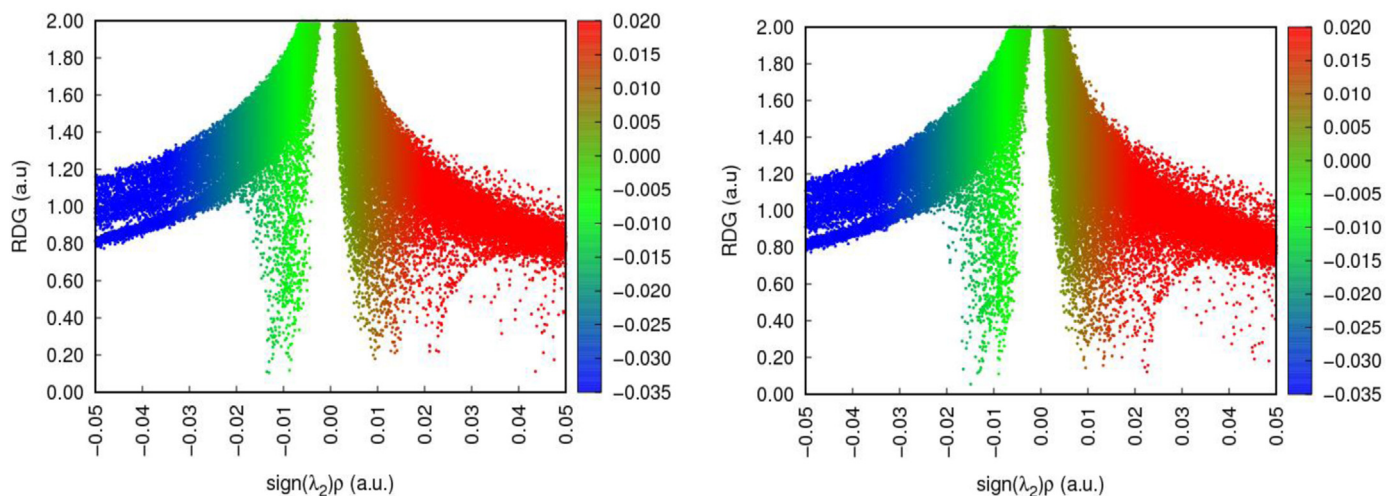


Fig. 15. Two-dimensional non-covalent-interaction analysis of thiazoles.

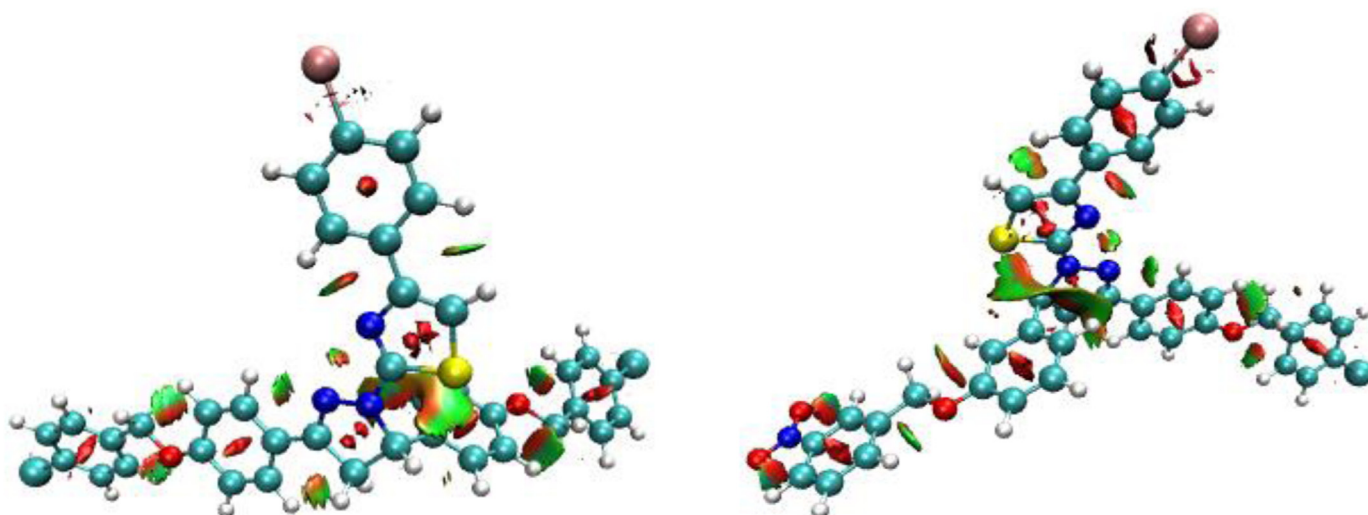


Fig. 16. Three-dimensional isosurfaces of non-covalent-interactions for thiazoles.

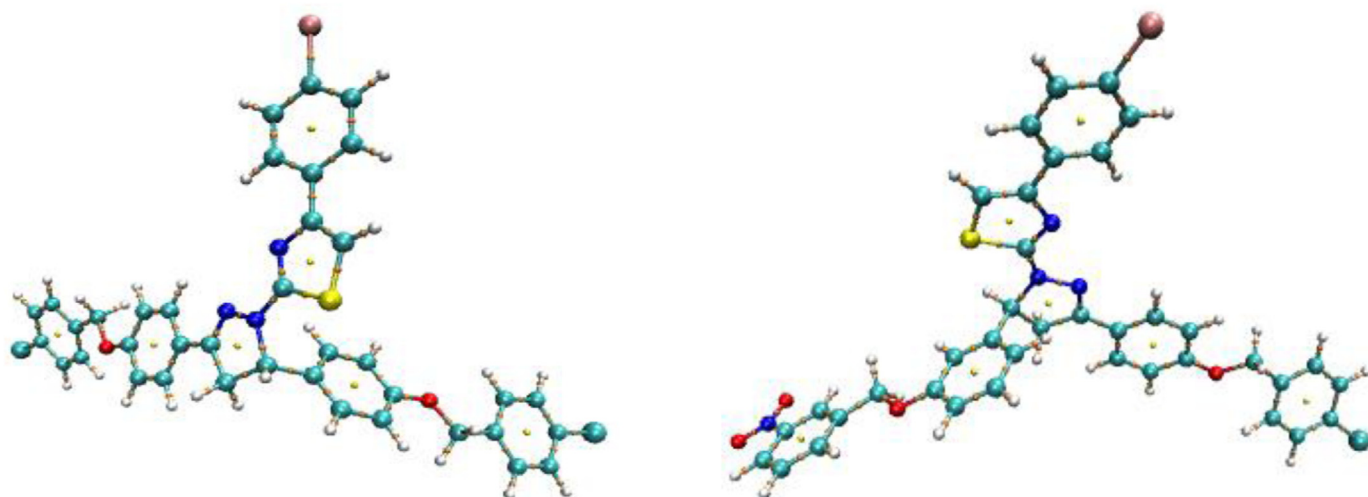


Fig. 17. Interacting paths and bond critical points for thiazoles.

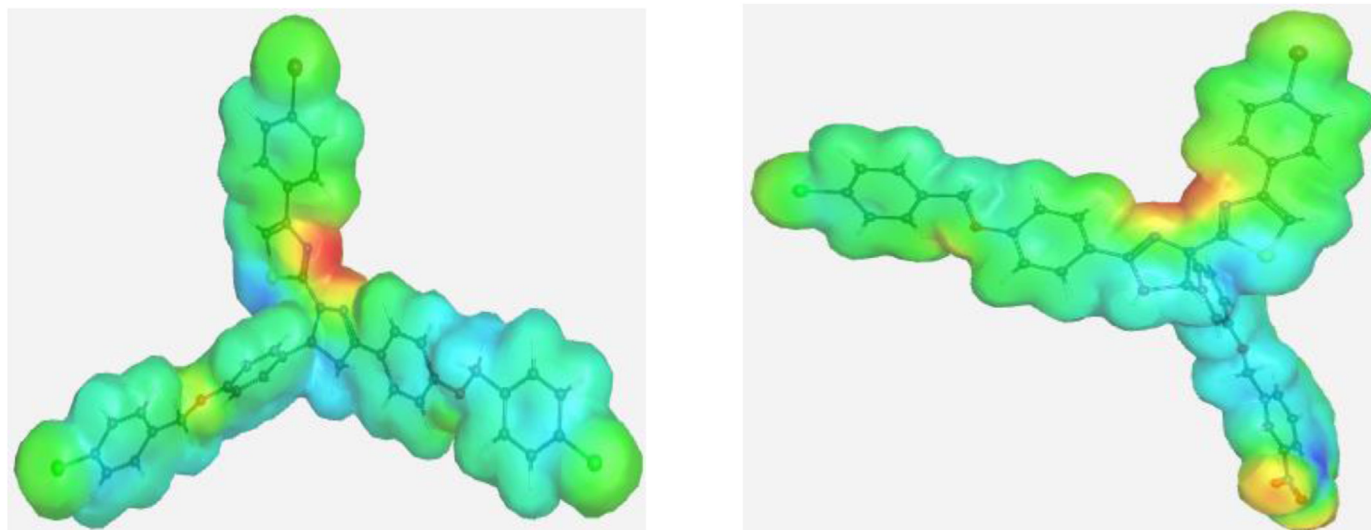


Fig. 18. Molecular electrostatic potential of thiazoles.

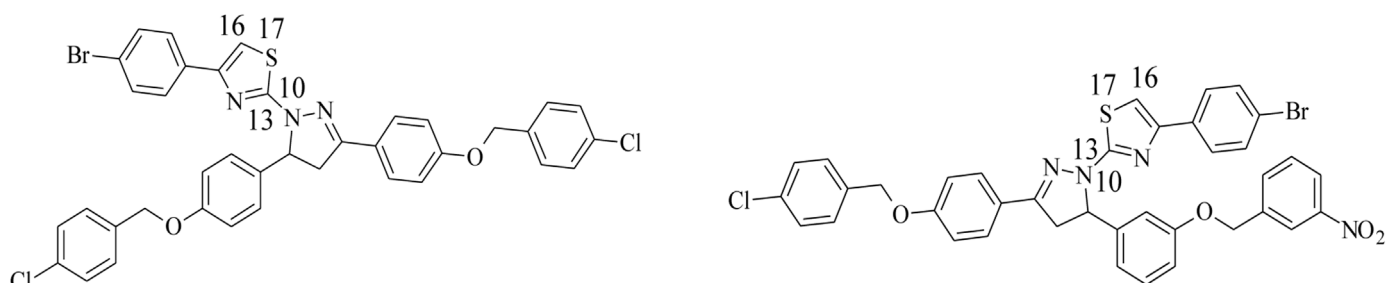


Fig. 19. Atomic labels for thiazoles.

Table 8
Conceptual density functional parameters for **11a-b**.

Atom	f^-		f^+		f^0		CDD	
	11a	11b	11a	11b	11a	11b	11a	11b
N10	0.0648	0.0636	0.0057	0.0028	0.0352	0.0332	-0.0591	-0.0608
C13	0.0153	0.0152	0.0172	0.0079	0.0162	0.0116	0.0019	-0.0074
S17	0.0928	0.0928	0.0586	0.0213	0.0757	0.0570	-0.0342	-0.0715

2.12. Conceptual density functional theory (CDFT)

In addition to MEP analysis, conceptual density functional theory (CDFT) can also be used as a chemical descriptor to probe reactive sites on compounds. Moreover, the latter can locate atomic sites where radical attacks can occur, amongst other parameters, which includes local softness/hardness, local electrophilicity/nucleophilicity etc., making it a useful descriptor for both chemical and biological processes [69].

The reactive sites can be measured by the Fukui Function which is defined in Eq. (11)

$$f(\vec{r}) = \frac{\partial \rho}{\partial N} v(\vec{r}) = \left(\frac{\delta \mu}{\delta v \vec{r}} \right) N \quad (11)$$

The condensed Fukui Functions (f^- , f^+ and f^0) and charge density difference (CDD) are depicted in Table 2. The Fukui Function can be calculated with the following equations

$$f^+(\vec{r}) = q_r(N+1) - q_r(N) \quad (12)$$

for a nucleophilic attack

$$f^-(\vec{r}) = q_r(N) - q_r(N-1) \quad (13)$$

for an electrophilic attack

$$f^0(\vec{r}) = q_r(N+1) - q_r(N-1) \quad (14)$$

for a radical attack where CCD is the difference between $f^+(\vec{r})$ and $f^-(\vec{r})$ [8]. Other than C13 in **11a**, the f^- and f^+ values support with our observations for MEP analyses (Table 8). We also observe a high probability for a radical attack on S17 in **11a**. This further support our observation for the ALIE analysis on this atom. As radical attacks are an indicator of potential sites that can act as a broom that sweeps up reactive oxygen species (ROS), it acts as useful input for structure-activity relationships during molecular docking analysis.

3. Conclusion

Two thiazole-pyrazoline hybrids have been successfully synthesized and characterized by various spectroscopic techniques. The antimicrobial activity of these compounds was evaluated *in vitro* using the well diffusion method. The tested compounds showed excellent antibacterial activity against all bacteria tested. In particular, it was found that the synthesized compounds could inhibit *A. baumannii* at 32 and 16 $\mu\text{g/mL}$, respectively, compared

to ciprofloxacin which was ineffective. Moreover, compounds displayed significant antifungal activity against *C. albicans*. Molecular docking studies demonstrated that the greater effectiveness of compound **11b** was due to its stronger binding affinity to the gram-positive and gram-negative bacteria. DFT studies also indicate that compound **11b** had a lower HOMO-LUMO gap compared to **11a** thus justifying its greater biological activity. The dual antibacterial/antifungal activity presented by the good interaction of the two tested compounds with bacteria and fungus can be explained by the co-presence of two antifungal pharmacophore sites ($X^{\delta-}$, $Y^{\delta-}$) where (X, Y) = (N, N) and (N, S) but the antibacterial pharmacophore site (N, NH) should be regenerated *in situ* via interaction folic acid with nitrogen atoms. Hence, the identified most active compound, by using POM Theory, may be considered as lead for further study in the search of novel pathogenic microorganisms inhibitory agent. The right formulation will be needed to improve the drug-like properties of these compounds, especially their lipophilicity and solubility.

4. Experimental part

4.1. Synthesis of hybrids (11a-b)

A mixture of pyrazoline derivatives (**9a-b**) (1 mmol), 4-bromophenacyl bromide **10** (0.83 gm, 3 mmol) and absolute ethanol (10 mL, 99.9%) was refluxed with stirring for (1–4 h) until completion the reaction which was monitored by TLC. The precipitate was isolated by suction filtration, washed with ethanol, dried and purified by recrystallization from toluene as a suitable solvent.

4.2. 2-(3,5-bis(4-((4-chlorobenzyl)oxy)phenyl)-4,5-dihydro-1H-pyrazol-1-yl)-4-(4-bromophenyl)thiazole (11a)

Yellow; m.p.: 217.1–219.3 °C; yield: 95.9%; $R_f = 0.49$ in *n*-Hex:EtOAc (2:3); FT-IR (KBr) (ν_{\max} / cm^{-1}): 1606 (C = C), 1548 (C = N); UV $\lambda_{\max} = 218$ nm; $^1\text{H NMR}$ (400 MHz, CDCl_3) (ppm): δ 3.32 (1H, dd, CH_2), 3.83 (1H, dd, CH_2), 5.01 (2H, s, OCH_2), 5.10 (2H, s, OCH_2), 5.59 (1H, d, CH), 6.81 (1H, s, CH), 6.92–7.73 (20H, m, Ar-H); $^{13}\text{C NMR}$ (100 MHz, CDCl_3) (ppm): δ 165.15 (C22), 159.83 (C6), 158.04 (C16), 151.53 (C10), 150.31 (C23), 135.39 (C4), 134.99 (C18), 134.34 (C13), 133.94 (C1), 133.74 (C21), 131.44 (C27 and C27'), 129.01 (C25), 128.82 (C8 and C8'), 128.73 (C26 and C26'), 128.20 (C2, C2', C20 and C20'), 127.98 (C3, C3', C19 and C19'), 127.42 (C14 and C14'), 124.58 (C9), 121.18 (C28), 115.03 (C7 and C7'), 114.89 (C15 and C15'), 103.57 (C24), 69.28 (C5), 69.22 (C17), 64.05 (C12), 43.51 (C11).

4.3. 4-(4-bromophenyl)-2-(3-(4-((4-chlorobenzyl)oxy)phenyl)-5-(3-((3-nitrobenzyl)oxy)phenyl)-4,5-dihydro-1H-pyrazol-1-yl)thiazole (11b)

Brown; m.p.: 144.7–146.3 °C; yield: 88.6%; $R_f = 0.43$ in *n*-Hex:EtOAc (2:3); FT-IR (KBr) (ν_{\max} / cm^{-1}): 1606 (C = C), 15,550 (C = N); UV $\lambda_{\max} = 218$ nm; $^1\text{H NMR}$ (400 MHz, CDCl_3) (ppm): δ 3.29 (1H, dd, CH_2), 3.86 (1H, dd, CH_2), 5.57 (4H, m, 2XOCH_2), 5.62 (1H, d, CH), 6.77 (1H, s, CH), 6.88–8.25 (20H, m, Ar-H); $^{13}\text{C NMR}$ (100 MHz, CDCl_3) (ppm): δ 165.12 (C26), 159.94 (C6), 158.52 (C15), 151.61 (C10), 150.35 (C22), 148.40 (C27), 143.65 (C13), 139.08 (C20), 135.03 (C4), 134.01 (C1), 133.95 (C25), 133.11 (C29), 131.48 (C31 and C31'), 129.94 (C8 and C8'), 129.54 (C24), 128.88 (C30 and C30'), 128.80 (C17), 128.05 (C2 and C2'), 127.46 (C3 and C3'), 124.47 (C9), 122.91 (C21), 122.11 (C23), 121.26 (C32), 119.85 (C18), 115.10 (C7 and C7'), 114.09 (C16), 113.00 (C14), 103.75 (C28), 69.33 (C5), 68.69 (C19), 64.42 (C12), 43.56 (C11).

4.4. Antimicrobial activity

4.4.1. Microbial strains tested

The antimicrobial activity of compounds (**11a-b**) was performed against four bacterial strains (*Staphylococcus aureus*, *E. coli*, *Pseudomonas aeruginosa*, and *Acinetobacter baumannii*) and against one fungal strain (*Candida albicans*), derived from hospitalized patients. The test organisms were validated with 0.5 MacFarland turbidity equivalents.

4.5. Well diffusion method

The evaluation of the antimicrobial activity of the synthesized compounds was performed *via* the well-diffusion technique, as screening test [70]. In this study, an MH (Mueller-Hinton) agar and potato dextrose agar was seeded in Petri dishes with the four selected bacterial strains and the one fungal strain, respectively. The newly synthesized compounds were prepared as a stock solution of 1000 μg /mL concentration in 5% DMSO solvent. Wells in the solid culture media (6 mm diameter) were impregnated with 20 μl of the tested compounds. Fungal and bacterial strains were incubated at 30 °C and 37 °C, respectively. For all studied microorganism strains, the diameter of inhibition and the inhibition percentage was measured after 24 h as well as after 48 h for *C. albicans*. The standard drug used was ciprofloxacin and fluconazole as a positive control and 5% DMSO as a negative control.

4.6. Minimum inhibitory concentration (MIC)

The MIC of compounds (**11a-b**) against the four bacterial strains and the one fungal strain was determined utilizing the micro-dilution technique according to the method described by after 24 h of incubation for bacteria and 48 h for *C. albicans* at 37 °C and 30 °C, respectively and 200 rpm shaking incubator (LabTech) [71]. Serial dilutions of the tested compounds were prepared at different concentrations of 0.5, 1, 2, 4, 8, 16, and 32 $\mu\text{g}/\text{ml}$ in 96-well microtiter plates. Bacterial growth was determined using a microplate reader at 600 nm. All experiments were performed in triplicate. The lowest concentration that inhibited bacterial and fungal growth was taken as the MIC value.

4.7. Statistical analysis

The data are provided as mean value + standard deviation (mean + SD), and each experiment was conducted with three independent replications. For the MIC data's statistical analysis, linear regression was employed. The differences were verified as significant at $p < 0.05$.

4.8. Molecular docking details

The synthesized compounds were optimized using Spartan 14 software [72]. The optimized chemical compounds were converted to .pdb format in preparation for subjection to Autodock tool software which helped in converting the ligand in .pdb format to .pdbqt format for docking calculation [73]. Also, tyrosyl-tRNA synthetase (PDB ID: 1jjj) [32] (gram-positive bacteria), type IIA topoisomerase (PDB ID: 2xct) [74] (gram-negative bacteria) and CYP51 (sterol 14- α demethylase) (PDB: 3juv) [33] were downloaded from online protein database (protein data bank) and were treated by removing water molecules and any small molecules which were downloaded with the target receptors using pymol software and were saved in .pdb format. The clean receptors were further subjected to autodock tool software in order to locate the active site in the treated receptor and convert it to the acceptable format (.pdbqt) before docking calculation *via* autodock vina software [75].

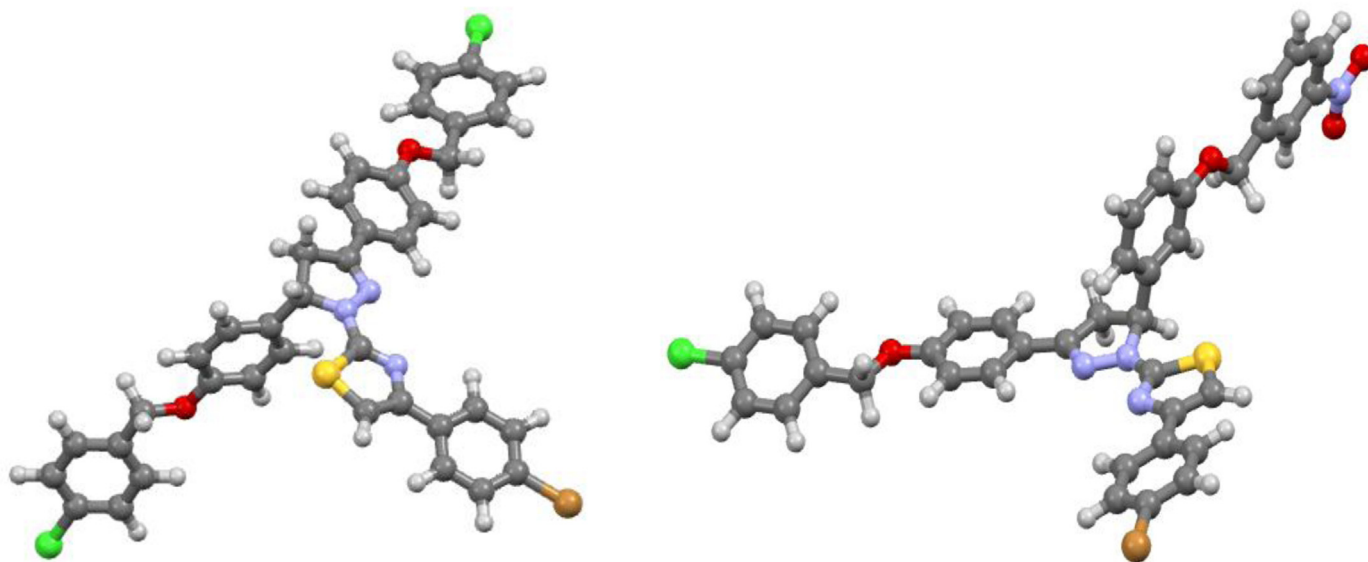


Fig. 20. Structures for thiazoles obtained from Mercury 2020.3.0.

4.9. DFT calculations

Thiazoles were constructed using Gaussian 09 software upon which they were subjected to conformer searches through molecular mechanics (MM) using Avogadro software. After obtaining their lowest conformers, optimization was performed at HF/6-31+Gdp, B3LYP-gD3/6-311++G(d,p) and M06-2X/6-311++G(d,p) level of theory using Gaussian 09 software [76]. Frequency calculations were carried out together with the optimized structures so that minimal conformation energies were obtained [77]. The optimized structures are shown in Fig. 20. From these optimized structures, fchk files were created, which were used as input for multiwfn [78], VMD [79] and gnuplot [80] software to carry out quantum theory of atoms in molecules (QTAIM) analysis, perform conceptual density functional theory (CDFT), molecular electrostatic potentials (MEP) and reveal non-covalent interactions (NCI). In addition to this, multiwfn software as also used to obtain, electron localization function (ELF), localized orbital locator (LOL) and average local ionization energies (ALIE) [81–83].

Credit author statement

Farouq Emam Hawaiz, Faisal A. Almalki and Narmin Hamaamin Hussien: Theoretical, experimental analysed, characterizations and interpreted the data; contributed analysis tools and data; wrote paper.

Aso Hameed Hasan and Taibi Ben Hadda: Coordinated the analysis tools and data; wrote paper.

Rezan Huseen Hama Salih and Adedapo S. Adeyinka: Synthesis part.

Taibi Ben Hadda, Louis-Charl C. Coetzee and Abel Kolawole Oye-bamiji: Computational parts.

Aso Hameed Hasan, Taibi Ben Hadda and Joazaizulfazli Jamalil: Analysed and checked the validity of data.

Declaration of Competing Interest

The authors declare that they have no known competing financial interests or personal relationships that could have appeared to influence the work reported in this paper.

Data availability

Data will be made available on request.

Acknowledgment

The authors wish to thank Universiti Teknologi Malaysia and the Ministry of Higher Education (MOHE) Malaysia for funding this research under the Fundamental Research Grant Scheme (FRGS/1/2022/STG04/UTM/02/4). Faisal A. Almalki would like to thank the Deanship of Scientific Research at Umm Al-Qura University for supporting this work by Grant Code: (22UQU4290462DSR02).

Supplementary materials

Supplementary material associated with this article can be found, in the online version, at doi:[10.1016/j.molstruc.2023.135191](https://doi.org/10.1016/j.molstruc.2023.135191).

References

- [1] D. Garella, E. Borretto, A. Di Stilo, K. Martina, G. Cravotto, P. Cintas, Microwave-assisted synthesis of N-heterocycles in medicinal chemistry, *Medchemcomm* 4 (10) (2013) 1323–1343, doi:[10.1039/C3MD00152K](https://doi.org/10.1039/C3MD00152K).
- [2] V.K. Mishra, M. Mishra, V. Kashaw, S.K. Kashaw, Synthesis of 1,3,5-trisubstituted pyrazolines as potential antimalarial and antimicrobial agents, *Bioorg. Med. Chem.* 25 (6) (2017) 1949–1962, doi:[10.1016/j.bmc.2017.02.025](https://doi.org/10.1016/j.bmc.2017.02.025).
- [3] A.H. Hasan, S.I. Amran, F.H. Saeed Hussain, B.A. Jaff, J. Jamalil, Molecular docking and recent advances in the design and development of cholinesterase inhibitor scaffolds: coumarin hybrids, *ChemistrySelect* 4 (48) (2019) 14140–14156, doi:[10.1002/slct.201903607](https://doi.org/10.1002/slct.201903607).
- [4] O.O. Tolu-Bolaji, S.O. Sojini, A.P. Okedere, O.O. Ajani, A review on the chemistry and pharmacological properties of benzodiazepine motifs in drug design, *Arab J. Basic Appl. Sci.* 29 (1) (2022) 287–306, doi:[10.1080/25765299.2022.2117677](https://doi.org/10.1080/25765299.2022.2117677).
- [5] E.I. Klimova, M. Martínez García, T. Klimova Berestneva, C. Alvarez Toledano, R. Alfredo Toskano, L. Ruiz Ramírez, The structure of bicyclic ferrocenylmethylene substituted 2-pyrazolines and their reactions with azodicarboxylic acid N-phenylimide, *J. Organomet. Chem.* 585 (1) (1999) 106–114, doi:[10.1016/S0022-328X\(99\)00202-8](https://doi.org/10.1016/S0022-328X(99)00202-8).
- [6] D. Havrylyuk, O. Roman, R. Lesyk, Synthetic approaches, structure activity relationship and biological applications for pharmacologically attractive pyrazole/pyrazoline–thiazolidine-based hybrids, *Eur. J. Med. Chem.* 113 (2016) 145–166, doi:[10.1016/j.ejmech.2016.02.030](https://doi.org/10.1016/j.ejmech.2016.02.030).
- [7] V. Chugh, G. Pandey, R. Rautela, C. Mohan, Heterocyclic compounds containing thiazole ring as important material in medicinal chemistry, *Mater. Today Proc.* 69 (2022) 478–481, doi:[10.1016/j.matpr.2022.09.150](https://doi.org/10.1016/j.matpr.2022.09.150).
- [8] M. Yusuf, P. Jain, Synthetic and biological studies of pyrazolines and related heterocyclic compounds, *Arabian J. Chem.* 7 (5) (2014) 553–596, doi:[10.1016/j.arabjc.2011.09.013](https://doi.org/10.1016/j.arabjc.2011.09.013).
- [9] M. Praceka, S. Megantara, R. Maharani, M. Muchtaridi, Comparison of various synthesis methods and synthesis parameters of pyrazoline derivatives, *J. Adv. Pharm. Technol. Res.* 12 (4) (2021) 321–326, doi:[10.4103/japtr.JAPTR_252_21](https://doi.org/10.4103/japtr.JAPTR_252_21).
- [10] A. Lévi, Synthesis of pyrazolines by the reactions of α,β -enones with diazomethane and hydrazines (review), *Chem. Heterocycl. Compd.* 33 (6) (1997) 647–659 (N Y), doi:[10.1007/BF02291794](https://doi.org/10.1007/BF02291794).

- [11] S. Eryilmaz, E. Türk Çelikoğlu, Ö. İdil, E. İnkaya, Z. Kozak, E. Mısır, M. Gül, Derivatives of pyridine and thiazole hybrid: synthesis, DFT, biological evaluation via antimicrobial and DNA cleavage activity, *Bioorg. Chem.* 95 (2020) 103476, doi:[10.1016/j.bioorg.2019.103476](https://doi.org/10.1016/j.bioorg.2019.103476).
- [12] M. Asad, M.N. Arshad, M. Oves, M. Khalid, S.A. Khan, A.M. Asiri, M. Rehan, H. Dzudzevic-Cancar, N-Trifluoroacetylated pyrazolines: synthesis, characterization and antimicrobial studies, *Bioorg. Chem.* 99 (2020) 103842, doi:[10.1016/j.bioorg.2020.103842](https://doi.org/10.1016/j.bioorg.2020.103842).
- [13] M.Y. Wani, A.R. Bhat, A. Azam, D.H. Lee, I. Choi, F. Athar, Synthesis and in vitro evaluation of novel tetrazole embedded 1,3,5-trisubstituted pyrazoline derivatives as *Entamoeba histolytica* growth inhibitors, *Eur. J. Med. Chem.* 54 (2012) 845–854, doi:[10.1016/j.ejmech.2012.03.049](https://doi.org/10.1016/j.ejmech.2012.03.049).
- [14] K. Cheng, J.-Y. Xue, H.-L. Zhu, Design, synthesis and antibacterial activity studies of thiazole derivatives as potent eCKAS III inhibitors, *Bioorg. Med. Chem. Lett.* 23 (14) (2013) 4235–4238, doi:[10.1016/j.bmcl.2013.05.006](https://doi.org/10.1016/j.bmcl.2013.05.006).
- [15] D. Kaminsky, G.J.M. Den Hartog, M. Wojtyra, M. Lelyukh, A. Gzella, A. Bast, R. Lesyk, Antifibrotic and anticancer action of 5-ene amino/iminothiazolidinones, *Eur. J. Med. Chem.* 112 (2016) 180–195, doi:[10.1016/j.ejmech.2016.02.011](https://doi.org/10.1016/j.ejmech.2016.02.011).
- [16] A. Pyrih, M. Jaskolski, A.K. Gzella, R. Lesyk, Synthesis, structure and evaluation of anticancer activity of 4-amino-1,3-thiazolinone/pyrazoline hybrids, *J. Mol. Struct.* 1224 (2021) 129059, doi:[10.1016/j.molstruc.2020.129059](https://doi.org/10.1016/j.molstruc.2020.129059).
- [17] M. Rana, R. Arif, F.I. Khan, V. Maurya, R. Singh, M.I. Faizan, S. Yasmeen, S.H. Dar, R. Alam, A. Sahu, T. Ahmad, Rahisuddin, Pyrazoline analogs as potential anticancer agents and their apoptosis, molecular docking, MD simulation, DNA binding and antioxidant studies, *Bioorg. Chem.* 108 (2021) 104665, doi:[10.1016/j.bioorg.2021.104665](https://doi.org/10.1016/j.bioorg.2021.104665).
- [18] R.A. Hassan, S.H. Emam, D. Hwang, G.-D. Kim, S.O. Hassanin, M.G. Khalil, A.M. Abdou, A. Sonousi, Design, synthesis and evaluation of anticancer activity of new pyrazoline derivatives by down-regulation of VEGF: molecular docking and apoptosis inducing activity, *Bioorg. Chem.* 118 (2022) 105487, doi:[10.1016/j.bioorg.2021.105487](https://doi.org/10.1016/j.bioorg.2021.105487).
- [19] F.W. Bell, A.S. Cantrell, M. Högberg, S.R. Jaskunas, N.G. Johansson, C.L. Jordan, M.D. Kinnick, P. Lind, J.M. Morin, R. Noréen, B. Öberg, J.A. Palkowitz, C.A. Parrish, P. Pranc, C. Sahibberg, R.J. Temansky, R.T. Vasileff, L. Vrang, S.J. West, H. Zhang, X.X. Zhou, Phenethylthiazolethiourea (PETT) Compounds, a New Class of HIV-1 Reverse Transcriptase Inhibitors. 1. Synthesis and Basic Structure-Activity Relationship Studies of PETT Analogs, *J. Med. Chem.* 38 (25) (1995) 4929–4936, doi:[10.1021/jm00025a010](https://doi.org/10.1021/jm00025a010).
- [20] P.K. Sharma, S.N. Sawhney, A. Gupta, G.B. Singh, S. Bani, Synthesis and anti-inflammatory activity of some 3-(2-thiazolyl)-1,2-benzisothiazoles, *Indian J. Chem. - Sect. B Org. Med. Chem.* 37 (4) (1998) 376–381.
- [21] I. Apostolidis, K. Liaras, A. Geronikaki, D. Hadjipavlou-Litina, A. Gavalas, M. Soković, J. Glamočija, A. Ćirić, Synthesis and biological evaluation of some 5-arylidene-2-(1,3-thiazol-2-ylimino)-1,3-thiazolidin-4-ones as dual anti-inflammatory/antimicrobial agents, *Bioorg. Med. Chem.* 21 (2) (2013) 532–539, doi:[10.1016/j.bmc.2012.10.046](https://doi.org/10.1016/j.bmc.2012.10.046).
- [22] J. Jacob P, S.L. Manju, Identification and development of thiazole leads as COX-2/5-LOX inhibitors through *in-vitro* and *in-vivo* biological evaluation for anti-inflammatory activity, *Bioorg. Chem.* 100 (2020) 103882, doi:[10.1016/j.bioorg.2020.103882](https://doi.org/10.1016/j.bioorg.2020.103882).
- [23] E.D. Dincel, E. Gürsoy, T. Yilmaz-Ozden, N. Ulusoy-Güzeldemirci, Antioxidant activity of novel imidazo[2,1-b]thiazole derivatives: design, synthesis, biological evaluation, molecular docking study and *in silico* ADME prediction, *Bioorg. Chem.* 103 (2020) 104220, doi:[10.1016/j.bioorg.2020.104220](https://doi.org/10.1016/j.bioorg.2020.104220).
- [24] S. Liu, R. Shang, L. Shi, D.C.-C. Wan, H. Lin, Synthesis and biological evaluation of 7H-thiazolo[3,2-b]-1,2,4-triazin-7-one derivatives as dual binding site acetylcholinesterase inhibitors, *Eur. J. Med. Chem.* 81 (2014) 237–244, doi:[10.1016/j.ejmech.2014.05.020](https://doi.org/10.1016/j.ejmech.2014.05.020).
- [25] Z.-Q. Sun, L.-X. Tu, F.-J. Zhuo, S.-X. Liu, Design and discovery of Novel Thiazole acetamide derivatives as anticholinesterase agent for possible role in the management of Alzheimer's, *Bioorg. Med. Chem. Lett.* 26 (3) (2016) 747–750, doi:[10.1016/j.bmcl.2016.01.001](https://doi.org/10.1016/j.bmcl.2016.01.001).
- [26] T.L. Schultz, C.P. Hencken, L.E. Woodard, G.H. Posner, R.H. Yolken, L. Jones-Brando, V.B. Carruthers, A thiazole derivative of artemisinin moderately reduces *Toxoplasma gondii* cyst burden in infected mice, *J. Parasitol.* 100 (4) (2014) 516–521, doi:[10.1645/13-451.1](https://doi.org/10.1645/13-451.1).
- [27] R.S. Joshi, P.G. Mandhane, S.D. Diwakar, S.K. Dabhade, C.H. Gill, Synthesis, analgesic and anti-inflammatory activities of some novel pyrazolines derivatives, *Bioorg. Med. Chem. Lett.* 20 (12) (2010) 3721–3725, doi:[10.1016/j.bmcl.2010.04.082](https://doi.org/10.1016/j.bmcl.2010.04.082).
- [28] S. Viveka, P.S. Dinesha, G.K. Nagaraja, S. Ballav, S. Kerkar, Design and synthesis of some new pyrazolyl-pyrazolines as potential anti-inflammatory, analgesic and antibacterial agents, *Eur. J. Med. Chem.* 101 (2015) 442–451, doi:[10.1016/j.ejmech.2015.07.002](https://doi.org/10.1016/j.ejmech.2015.07.002).
- [29] S. Mor, M. Khatri, Synthesis, antimicrobial evaluation, α -amylase inhibitory ability and molecular docking studies of 3-alkyl-1-(4-(aryl/heteroaryl)thiazol-2-yl)indeno[1,2-c]pyrazol-4(1H)-ones, *J. Mol. Struct.* 1249 (2022) 131526, doi:[10.1016/j.molstruc.2021.131526](https://doi.org/10.1016/j.molstruc.2021.131526).
- [30] S.I. Eissa, A.M. Farrag, S.Y. Abbas, M.F. El Shehry, A. Ragab, E.A. Fayed, Y.A. Ammar, Novel structural hybrids of quinoline and thiazole moieties: synthesis and evaluation of antibacterial and antifungal activities with molecular modeling studies, *Bioorg. Chem.* 110 (2021) 104803, doi:[10.1016/j.bioorg.2021.104803](https://doi.org/10.1016/j.bioorg.2021.104803).
- [31] R.H.H. Salih, A.H. Hasan, A.J. Hussein, M.K. Samad, S. Shakya, J. Jamalish, F.E. Hawaiz, M.R.F. Pratama, One-pot synthesis, molecular docking, ADMET, and DFT studies of novel pyrazolones as promising SARS-CoV-2 main protease inhibitors, *Res. Chem. Intermed.* 48 (2022) 4729–4751, doi:[10.1007/s11164-022-04831-5](https://doi.org/10.1007/s11164-022-04831-5).
- [32] X. Qiu, C.A. Janson, W.W. Smith, S.M. Green, P. McDevitt, K. Johanson, P. Carter, M. Hibbs, C. Lewis, A. Chalker, A. Fosberry, J. Lalonde, J. Berge, P. Brown, C.S.V. Houge-Frydrych, R.L. Jarvest, Crystal structure of Staphylococcus aureus tyrosyl-tRNA synthetase in complex with a class of potent and specific inhibitors, *Protein Sci.* 10 (10) (2001) 2008–2016, doi:[10.1110/ps.18001](https://doi.org/10.1110/ps.18001).
- [33] N. Strushkevich, S.A. Usanov, H.-W. Park, Structural basis of human CYP51 inhibition by antifungal azoles, *J. Mol. Biol.* 397 (4) (2010) 1067–1078, doi:[10.1016/j.jmb.2010.01.075](https://doi.org/10.1016/j.jmb.2010.01.075).
- [34] N.H. Hussien, A.H. Hasan, J. Jamalish, S. Shakya, S. Chander, H. Kharkwal, S. Murugesan, V. Ajit Bastikar, P. Pyarelal Gupta, Potential inhibitory activity of phytoconstituents against black fungus: *in silico* ADMET, molecular docking and MD simulation studies, *Comput. Toxicol.* 24 (2022) 100247, doi:[10.1016/j.comtox.2022.100247](https://doi.org/10.1016/j.comtox.2022.100247).
- [35] A.H. Hasan, N.H. Hussien, S. Shakya, J. Jamalish, M.R.F. Pratama, S. Chander, H. Kharkwal, S. Murugesan, *In silico* discovery of multi-targeting inhibitors for the COVID-19 treatment by molecular docking, molecular dynamics simulation studies, and ADMET predictions, *Struct. Chem.* 33 (2022) 1645–1665, doi:[10.1007/s11224-022-01996-y](https://doi.org/10.1007/s11224-022-01996-y).
- [36] M. Anowar Hosen, N. Sultana Munia, M. Al-Ghorbani, M. Baashen, F.A. Almalki, T. Ben Hadda, F. Ali, S. Mahmud, M. Abu Saleh, H. Laaroussi, S.M.A. Kawsar, Synthesis, antimicrobial, molecular docking and molecular dynamics studies of lauroyl thymidine analogs against SARS-CoV-2: POM study and identification of the pharmacophore sites, *Bioorg. Chem.* 125 (2022) 105850, doi:[10.1016/j.bioorg.2022.105850](https://doi.org/10.1016/j.bioorg.2022.105850).
- [37] N.S. Munia, M.A. Hosen, K.M.A. Azzam, M. Al-Ghorbani, M. Baashen, M.K. Hossein, F. Ali, S. Mahmud, M.S.S. Shimu, F.A. Almalki, T.B. Hadda, H. Laaroussi, S. Naimi, S.M.A. Kawsar, Synthesis, antimicrobial, SAR, PASS, molecular docking, molecular dynamics and pharmacokinetics studies of 5'-O-uridine derivatives bearing acyl moieties: POM study and identification of the pharmacophore sites, *Nucleosides Nucleotides Nucleic Acids* 41 (10) (2022) 1036–1083, doi:[10.1080/15257770.2022.2096898](https://doi.org/10.1080/15257770.2022.2096898).
- [38] S.A. Majid, J.M. Mir, M.A. Bhat, A.H. Shalla, A. Pandey, T.B. Hadda, M.H. Abdel-lattif, A pair of carbazate derivatives as novel Schiff base ligands: DFT and POM theory supported spectroscopic and biological evaluation, *J. Biomol. Struct. Dyn.* (2022) 1–17, doi:[10.1080/07391102.2022.2090437](https://doi.org/10.1080/07391102.2022.2090437).
- [39] M. Rbaa, S. Haida, B. Tuzun, A. Hichar, A.E. Hassane, A. Kribii, Y. Lakhri, T.B. Hadda, A. Zarrouk, B. Lakhri, E. Berdimurodov, Synthesis, characterization and bioactivity of novel 8-hydroxyquinoline derivatives: experimental, molecular docking, DFT and POM analyses, *J. Mol. Struct.* 1258 (2022) 132688, doi:[10.1016/j.molstruc.2022.132688](https://doi.org/10.1016/j.molstruc.2022.132688).
- [40] Y. Lakhri, M. Rbaa, B. Tuzun, A. Hichar, E.H. Anouar, K. Ounine, F. Almalki, T.B. Hadda, A. Zarrouk, B. Lakhri, Synthesis, structural confirmation, antibacterial properties and bio-informatics computational analyses of new pyrrrole based on 8-hydroxyquinoline, *J. Mol. Struct.* 1259 (2022) 132683, doi:[10.1016/j.molstruc.2022.132683](https://doi.org/10.1016/j.molstruc.2022.132683).
- [41] M. Chalkha, A. Nakkabi, T.B. Hadda, M. Berredjem, A.E. Moussaoui, M. Bakhouch, M. Saadi, L.E. Ammari, F.A. Almalki, H. Laaroussi, V. Jevtovic, M.E. Yazidi, Crystallographic study, biological assessment and POM/Docking studies of pyrazoles-sulfonamide hybrids (PSH): identification of a combined Antibacterial/Antiviral pharmacophore sites leading to *in-silico* screening the anti-Covid-19 activity, *J. Mol. Struct.* 1267 (2022) 133605, doi:[10.1016/j.molstruc.2022.133605](https://doi.org/10.1016/j.molstruc.2022.133605).
- [42] K. Bechlem, M. Berredjem, S.E. Djouad, T.O. Sothea, S. Bouacida, C. Marminon, T.B. Hadda, J. Lebreton, A. Bouzina, Novel N-acylsulfamoyl-oxazolodin-2ones: synthesis, antitumor activity, X-ray crystallographic study, molecular docking and POM analyses, *J. Mol. Struct.* 1262 (2022) 132935, doi:[10.1016/j.molstruc.2022.132935](https://doi.org/10.1016/j.molstruc.2022.132935).
- [43] S. Akkoc, H. Karatas, M.T. Muhammed, Z. Kökbudak, A. Ceylan, F. Almalki, H. Laaroussi, T. Ben Hadda, Drug design of new therapeutic agents: molecular docking, molecular dynamics simulation, DFT and POM analyses of new Schiff base ligands and impact of substituents on bioactivity of their potential antifungal pharmacophore site, *J. Biomol. Struct. Dyn.* (2022) 1–14, doi:[10.1080/07391102.2022.2111360](https://doi.org/10.1080/07391102.2022.2111360).
- [44] T. Koopmans, Über die Zuordnung von Wellenfunktionen und Eigenwerten zu den Einzelnen Elektronen Eines Atoms, *Physica* 1 (1) (1934) 104–113, doi:[10.1016/S0031-8914\(34\)90011-2](https://doi.org/10.1016/S0031-8914(34)90011-2).
- [45] L.R. Domingo, M. Ríos-Gutiérrez, P. Pérez, Applications of the conceptual density functional theory indices to organic chemistry reactivity, *Molecules* 21 (6) (2016) 748, doi:[10.3390/molecules21060748](https://doi.org/10.3390/molecules21060748).
- [46] R.G. Parr, R.G. Pearson, Absolute hardness: companion parameter to absolute electronegativity, *J. Am. Chem. Soc.* 105 (26) (1983) 7512–7516, doi:[10.1021/ja00364a005](https://doi.org/10.1021/ja00364a005).
- [47] R.G. Pearson, Absolute electronegativity and hardness: application to inorganic chemistry, *Inorg. Chem.* 27 (4) (1988) 734–740, doi:[10.1021/ic00277a030](https://doi.org/10.1021/ic00277a030).
- [48] R.K. Roy, S. Krishnamurti, P. Geerlings, S. Pal, Local softness and hardness based reactivity descriptors for predicting intra- and intermolecular reactivity sequences: carbonyl compounds, *J. Phys. Chem. A* 102 (21) (1998) 3746–3755, doi:[10.1021/jp973450v](https://doi.org/10.1021/jp973450v).
- [49] P.K. Chattaraj, S. Giri, Electrophilicity index within a conceptual DFT framework, *Ann. Rep. Sect. "C" (Phys. Chem.)* 105 (0) (2009) 13–39, doi:[10.1039/B802832j](https://doi.org/10.1039/B802832j).
- [50] P.K. Chattaraj, U. Sarkar, D.R. Roy, Electrophilicity index, *Chem. Rev.* 106 (6) (2006) 2065–2091, doi:[10.1021/cr040109f](https://doi.org/10.1021/cr040109f).

- [51] R.G. Parr, L.V. Szentpály, S. Liu, Electrophilicity index, *J. Am. Chem. Soc.* 121 (9) (1999) 1922–1924, doi:10.1021/ja983494x.
- [52] C.–G. Zhan, J.A. Nichols, D.A. Dixon, Ionization potential, electron affinity, electronegativity, hardness, and electron excitation energy: molecular properties from density functional theory orbital energies, *J. Phys. Chem. A* 107 (20) (2003) 4184–4195, doi:10.1021/jp0225774.
- [53] R.G. Pearson, Absolute electronegativity and hardness correlated with molecular orbital theory, *Proc. Natl. Acad. Sci.* 83 (22) (1986) 8440–8441, doi:10.1073/pnas.83.22.8440.
- [54] R.G. Parr, W. Yang, Density-functional theory of the electronic structure of molecules, *Annu. Rev. Phys. Chem.* 46 (1) (1995) 701–728, doi:10.1146/annurev.pc.46.100195.003413.
- [55] A.T. Maynard, M. Huang, W.G. Rice, D.G. Covell, Reactivity of the HIV-1 nucleocapsid protein p7 zinc finger domains from the perspective of density-functional theory, *Proc. Natl. Acad. Sci.* 95 (20) (1998) 11578–11583, doi:10.1073/pnas.95.20.11578.
- [56] R. Parthasarathi, V. Subramanian, D.R. Roy, P.K. Chattaraj, Electrophilicity index as a possible descriptor of biological activity, *Bioorg. Med. Chem.* 12 (21) (2004) 5533–5543, doi:10.1016/j.bmc.2004.08.013.
- [57] L.R. Domingo, P. Pérez, The nucleophilicity N index in organic chemistry, *Org. Biomol. Chem.* 9 (20) (2011) 7168–7175, doi:10.1039/C1OB05856H.
- [58] D.F.V. Lewis, C. Ioannides, D.V. Parke, Interaction of a series of nitriles with the alcohol-inducible isoform of P450: computer analysis of structure-activity relationships, *Xenobiotica* 24 (5) (1994) 401–408, doi:10.3109/00498259409043243.
- [59] F.A. Bulat, J.S. Murray, P. Politzer, Identifying the most energetic electrons in a molecule: the highest occupied molecular orbital and the average local ionization energy, *Comput. Theor. Chem.* 1199 (2021) 113192, doi:10.1016/j.comptc.2021.113192.
- [60] M. Kandasamy, G. Velraj, Ab initio/DFT electronic structure calculations, spectroscopic studies of 5-bromo-2-pyridinecarbonitrile – a comparative study, *Solid State Sci.* 14 (8) (2012) 1071–1079, doi:10.1016/j.solidstatesciences.2012.05.003.
- [61] A. Innasiraj, B. Anandhi, Y. Gnanadeepam, N. Das, F. Paularokiadoss, A.V. Ilavarasi, C.D. Sheela, D.R. Ampasala, T.C. Jayakumar, Experimental and theoretical studies of novel Schiff base based on diammino benzophenone with formyl chromone – BPAMC, *J. Mol. Struct.* 1265 (2022) 133450, doi:10.1016/j.molstruc.2022.133450.
- [62] P. Politzer, J.S. Murray, F.A. Bulat, Average local ionization energy: a review, *J. Mol. Model.* 16 (11) (2010) 1731–1742, doi:10.1007/s00894-010-0709-5.
- [63] L.-C.C. Coetzee, A.S. Adeyinka, N. Magwa, A theoretical evaluation of the efficiencies of metal-free 1,3,4-oxadiazole dye-sensitized solar cells: insights from electron-hole separation distance analysis, *Energies* 15 (13) (2022) 4913, doi:10.3390/en15134913.
- [64] P. Fuentealba, E. Chamorro, J.C. Santos, Chapter 5 Understanding and using the electron localization function, in: A. Toro-Labbé (Ed.), *Theoretical and Computational Chemistry*, Elsevier, 2007, pp. 57–85.
- [65] H.L. Schmider, A.D. Becke, Chemical content of the kinetic energy density, *J. Mol. Struct. Theor. Chem.* 527 (1) (2000) 51–61, doi:10.1016/S0166-1280(00)00477-2.
- [66] R. Chaudret, B. de Courcy, J. Contreras-García, E. Gloaguen, A. Zehnacker-Rentien, M. Mons, J.P. Piquemal, Unraveling non-covalent interactions within flexible biomolecules: from electron density topology to gas phase spectroscopy, *Phys. Chem. Chem. Phys.* 16 (21) (2014) 9876–9891, doi:10.1039/C3CP52774C.
- [67] P.L.A. Popelier, On the full topology of the Laplacian of the electron density, *Coord. Chem. Rev.* 197 (1) (2000) 169–189, doi:10.1016/S0010-8545(99)00189-7.
- [68] I. Kostova, N. Trendafilova, G. Momekov, Theoretical and spectroscopic evidence for coordination ability of 3,3'-benzylidenedi-4-hydroxycoumarin. New neodymium (III) complex and its cytotoxic effect, *J. Inorg. Biochem.* 99 (2) (2005) 477–487, doi:10.1016/j.jinorgbio.2004.10.022.
- [69] H.E. Hashem, E.A. Mohamed, A.A. Farag, N.A. Negm, E.A.M. Azmy, New heterocyclic Schiff base-metal complex: synthesis, characterization, density functional theory study, and antimicrobial evaluation, *Appl. Organomet. Chem.* 35 (9) (2021) e6322, doi:10.1002/aoc.6322.
- [70] F.D. Gonelimali, J. Lin, W. Miao, J. Xuan, F. Charles, M. Chen, S.R. Hatab, Antimicrobial properties and mechanism of action of some plant extracts against food pathogens and spoilage microorganisms, *Front. Microbiol.* 9 (2018), doi:10.3389/fmicb.2018.01639.
- [71] E.N. Okolo, D.I. Ugwu, B.E. Ezema, J.C. Ndefo, F.U. Eze, C.G. Ezema, J.A. Ezugwu, O.T. Ujam, New chalcone derivatives as potential antimicrobial and antioxidant agent, *Sci. Rep.* 11 (1) (2021) 21781, doi:10.1038/s41598-021-01292-5.
- [72] A.K. Oyebamiji, E.A. Soetan, S.A. Akintelu, A.O. Ayeleso, E. Mukwevho, Alpha-glucosidase activity of phytochemicals from *Phyllanthus amarus* leaves via in-silico approaches, *Pharmacol. Res. Mod. Chin. Med.* 2 (2022) 100054, doi:10.1016/j.prmcm.2022.100054.
- [73] A.H. Hasan, S. Murugesan, S.I. Amran, S. Chander, M.M. Alanazi, T.B. Hadda, S. Shakya, M.R.F. Pratama, B. Das, S. Biswas, J. Jamalis, Novel thiophene Chalcones-Coumarin as acetylcholinesterase inhibitors: design, synthesis, biological evaluation, molecular docking, ADMET prediction and molecular dynamics simulation, *Bioorg. Chem.* 119 (2022) 105572, doi:10.1016/j.bioorg.2021.105572.
- [74] B.D. Bax, P.F. Chan, D.S. Eggleston, A. Fosberry, D.R. Gentry, F. Gorrec, I. Giordano, M.M. Hann, A. Hennessy, M. Hibbs, J. Huang, E. Jones, J. Jones, K.K. Brown, C.J. Lewis, E.W. May, M.R. Saunders, O. Singh, C.E. Spitzfaden, C. Shen, A. Shillings, A.J. Theobald, A. Wohlkonig, N.D. Pearson, M.N. Gwynn, Type IIA topoisomerase inhibition by a new class of antibacterial agents, *Nature* 466 (7309) (2010) 935–940, doi:10.1038/nature09197.
- [75] A.H. Hasan, S. Shakya, F.H.S. Hussain, S. Murugesan, S. Chander, M.R.F. Pratama, S. Jamil, B. Das, S. Biswas, J. Jamalis, Design, synthesis, anti-acetylcholinesterase evaluation and molecular modelling studies of novel coumarin-chalcone hybrids, *J. Biomol. Struct. Dyn.* (2023) 1–13, doi:10.1080/07391102.2022.2162583.
- [76] G.W.T.M.J. Frisch, H.B. Schlegel, G.E. Scuseria, M.A. Robb, J.R. Cheeseman, G. Scalmani, V. Barone, G.A. Petersson, H. Nakatsuji, X. Li, M. Caricato, A. Marenich, J. Bloino, B.G. Janesko, R. Gomperts, B. Mennucci, H.P. Hratchian, J.V. Ortiz, A.F. Izmaylov, J.L. Sonnenberg, D. Williams-Young, F. Ding, F. Lipparini, F. Egidi, J. Goings, B. Peng, A. Petrone, T. Henderson, D. Ranasinghe, V.G. Zakrzewski, J. Gao, N. Rega, G. Zheng, W. Liang, M. Hada, M. Ehara, K. Toyota, R. Fukuda, J. Hasegawa, M. Ishida, T. Nakajima, Y. Honda, O. Kitao, H. Nakai, T. Vreven, K. Throssell, J.A. Montgomery Jr., J.E. Peralta, F. Ogliaro, M. Bearpark, J.J. Heyd, E. Brothers, K.N. Kudin, V.N. Staroverov, T. Keith, R. Kobayashi, J. Normand, K. Raghavachari, A. Rendell, J.C. Burant, S.S. Iyengar, J. Tomasi, M. Cossi, J.M. Millam, M. Klene, C. Adamo, R. Cammi, J.W. Ochterski, R.L. Martin, K. Morokuma, O. Farkas, J.B. Foresman, D.J. Fox, *Gaussian 09, Revision E.01*, Gaussian, Inc., Wallingford CT, 2009.
- [77] K. Anbukarasi, S. Xavier, A.H. Hasan, L.Y. Er, J. Jamalis, S. Sebastian, S. Periandy, DFT and molecular docking analysis of newly synthesized compound (2E)-3-[3-(Benzyloxy)phenyl]-1-(4'-chlorophenyl)-2-propen-1-one [Bpclpo], *Curr. Phys. Chem.* 13 (2023) 1–38, doi:10.2174/1877946812666220928102954.
- [78] T. Lu, F. Chen, Multiwfn: a multifunctional wavefunction analyzer, *J. Comput. Chem.* 33 (5) (2012) 580–592, doi:10.1002/jcc.22885.
- [79] W. Humphrey, A. Dalke, K. Schulten, VMD: visual molecular dynamics, *J. Mol. Graph.* 14 (1) (1996) 33–38, doi:10.1016/0263-7855(96)00018-5.
- [80] T. Williams and C. Kelly, (2023) Available from: <http://www.gnuplot.info/>.
- [81] Y.S. Mary, P.B. Miniyaar, Y.S. Mary, K.S. Resmi, C.Y. Panicker, S. Armaković, S.J. Armaković, R. Thomas, B. Sureshkumar, Synthesis and spectroscopic study of three new oxadiazole derivatives with detailed computational evaluation of their reactivity and pharmaceutical potential, *J. Mol. Struct.* 1173 (2018) 469–480, doi:10.1016/j.molstruc.2018.07.026.
- [82] S. Beegum, Y.S. Mary, Y.S. Mary, R. Thomas, S. Armaković, S.J. Armaković, J. Zitko, M. Dolezal, C. Van Alsenoy, Exploring the detailed spectroscopic characteristics, chemical and biological activity of two cyanopyrazine-2-carboxamide derivatives using experimental and theoretical tools, *Spectrochim. Acta Part A* 224 (2020) 117414, doi:10.1016/j.saa.2019.117414.
- [83] M. Hossain, R. Thomas, Y.S. Mary, K.S. Resmi, S. Armaković, S.J. Armaković, A.K. Nanda, G. Vijayakumar, C.V. Alsenoy, Understanding reactivity of two newly synthesized imidazole derivatives by spectroscopic characterization and computational study, *J. Mol. Struct.* 1158 (2018) 176–196, doi:10.1016/j.molstruc.2018.01.029.